Dynamics of the ssDNA Recognition by the RepA Hexameric Helicase of Plasmid RSF1010: Analyses Using Fluorescence Stopped-Flow Intensity and Anisotropy Methods

ARTICLE *in* JOURNAL OF MOLECULAR BIOLOGY · APRIL 2009

Impact Factor: 4.33 · DOI: 10.1016/j.jmb.2009.03.027 · Source: PubMed

5 AUTHORS, INCLUDING:

Iraida Andreeva
Virginia Polytechnic Institute and State Univ…
30 PUBLICATIONS **155** CITATIONS
SEE PROFILE

Michal R Szymanski
University of Texas Medical Branch at Galves…
26 PUBLICATIONS **137** CITATIONS
SEE PROFILE

Published in final edited form as:
J Mol Biol. 2009 May 15; 388(4): 751–775. doi:10.1016/j.jmb.2009.03.027.

Dynamics of the ssDNA Recognition by the RepA Hexameric Helicase of Plasmid RSF1010: Analyses Using Fluorescence Stopped-Flow Intensity and Anisotropy Methods☆

Iraida E. Andreeva, **Michal R. Szymanski**, **Maria J. Jezewska**, **Roberto Galletto**, and **Wlodzimierz Bujalowski***
Department of Biochemistry and Molecular Biology, The University of Texas Medical Branch at Galveston, 301 University Boulevard, Galveston, TX 77555-1053, USA

Department of Obstetrics and Gynecology, The University of Texas Medical Branch at Galveston, 301 University Boulevard, Galveston, TX 77555-1053, USA

Sealy Center for Structural Biology and Sealy Center for Cancer Cell Biology, The University of Texas Medical Branch at Galveston, 301 University Boulevard, Galveston, TX 77555-1053, USA

Abstract

The kinetic mechanism of the single-stranded DNA (ssDNA) recognition by the RepA hexameric replicative helicase of the plasmid RSF1010 and the nature of formed intermediates, in the presence of the ATP nonhydrolyzable analog, β,γ-imidoadenosine-5′-triphosphate (AMP-PNP), have been examined, using the fluorescence intensity and anisotropy stopped-flow and analytical ultracentrifugation methods. Association of the RepA hexamer with the ssDNA oligomers that engage the total DNA-binding site and exclusively the strong DNA-binding subsite is a minimum four-step mechanism

$$Helicase+ssDNA \underset{k_{-1}}{\overset{k_1}{\rightleftarrows}} (H-ssDNA)_1 \underset{k_{-2}}{\overset{k_2}{\rightleftarrows}} (H-ssDNA)_2 \underset{k_{-3}}{\overset{k_3}{\rightleftarrows}} (H-ssDNA)_3 \underset{k_{-4}}{\overset{k_4}{\rightleftarrows}} (H-ssDNA)_4$$

Extreme stability of the RepA hexamer precludes any disintegration of its structure, and the sequential character of the mechanism indicates that the enzyme exists in a predominantly single conformation prior to the association with the nucleic acid. Moreover, the hexameric helicase possesses a DNA-binding site located outside its cross channel. The reaction steps have dramatically different dynamics, with rate constants differing by 2–3 orders of magnitude. Such behavior indicates a very diverse nature of the observed transitions, which comprises binding steps and large conformational transitions of the helicase, including local opening of the hexameric structure. Steady-state fluorescence anisotropies of intermediates indicate that the entry of the DNA into the cross channel is initiated from the 5′ end of the bound nucleic acid. The global structure of the tertiary complex RepA–ssDNA–AMP–PNP is very different from the structure of the binary complex RepA–AMP-PNP, indicating that, in equilibrium, the RepA hexamer–ssDNA–AMP-PNP complex exists as a mixture of partially open states.

☆This work was supported by National Institutes of Health Grants GM46679 and GM58565 (to W.B.).

*Corresponding author. wbujalow@utmb.edu..
Present address: R. Galletto, Department of Biochemistry and Biophysics, Washington University, St. Louis, MO, USA.

Keywords

helicases; DNA replication; protein–ssDNA interactions; stopped-flow kinetics

Introduction

In the course of major processes of DNA and RNA metabolism, such as replication, recombination, repair, and translation, the duplex regions of the nucleic acid are transiently unwound, forming a metabolically active single-stranded DNA (ssDNA) intermediate.[1-7] The unwinding reaction is catalyzed by a class of enzymes called helicases and is fueled by the hydrolysis of nucleotide triphosphates. The RepA protein is a hexameric DNA replicative helicase that is essential for replication of RSF1010 plasmid, a broad-host nonconjugative plasmid that can confer bacterial resistance to sulfonamides and streptomycin.[8-11] What distinguishes the RepA protein from other hexameric helicases is that its ringlike hexameric structure is extremely stable without any cofactors or specific salt in solution.[8,9,12-14] The hexameric structure of the analogous *Escherichia coli* DnaB replicative helicase is stabilized only by Mg^{2+} cations.[15,16] However, several other well-known hexameric enzymes, such as bacteriophage T7, T4, or the *E. coli* transcription termination factor Rho helicases, assemble into the hexamer at physiological concentrations of the proteins, in the presence of nucleotide cofactors and/or the ssDNA.[17-20]

The RepA hexamer is the smallest known hexameric helicase with a molecular mass of ~180 kDa.[8-14] In the crystal structure, the diameter of a single RepA hexamer is ~115 Å, while the diameter of the central cross channel of the ringlike structure of the enzyme is only ~17 Å.[9] Nevertheless, analytical ultracentrifugation and dynamic light-scattering studies indicate that the global structure of the RepA hexamer in solution is significantly different from its crystal structure.[21] The axial ratio of the protein, modeled as an ellipsoid of revolution, is ~4.5 as compared to only ~2.4 for the crystal structure. The large axial ratio and the experimentally determined partial specific volume strongly suggest that, in solution, the diameter of the cross channel of the hexamer is larger than ~17 Å seen in the crystal. These studies also provided the first indication of a significant structural flexibility of the RepA hexamer. The enzyme exists in at least four global conformational states, modulated by the number of bound cofactors. Modulation of the global structure is separated into two phases, depending on the number of bound nucleotide cofactors. Nucleotide binding controls the helicase–ssDNA interactions, through the changes of the enzyme structure and its ssDNA affinity, prior to DNA binding.[21]

Interactions with the ssDNA conformation of the nucleic acid play a paramount role in the activities of all helicases.[1-7,12,16,21-27] Fluorescence energy transfer studies provide strong evidence that, in the complex with the ssDNA, the ssDNA passes through the central cross channel of the RepA hexamer.[28] Kinetic studies of the analogous DnaB helicase clearly indicate that the DNA enters the cross channel of ~40 Å in diameter, through the local opening of the hexameric structure.[29,30] However, the mechanism by which the nucleic acid enters the small cross channel of the extremely stable hexameric structure of the RepA helicase has never been addressed. Dynamics, energetics, and the nature of the formed intermediates are unknown. The total site size of the enzyme–ssDNA complex, that is, the total number of occluded nucleotides by the RepA hexamer in the complex, is 19±1 nucleotides, analogous to the site size of 20±3 nucleotides of the complex between much larger DnaB hexamer and the nucleic acid.[12,16,24-27] Moreover, similar to the DnaB helicase, the total ssDNA-binding site of the RepA hexamer is heterogeneous; that is, it contains strong and weak DNA-binding subsites, sequentially placed within the total binding site (Fig. 1). A similar presence of the strong and weak DNA-binding subsites has been

found for the monomeric *E. coli* PriA helicase, indicating that this is a general structure–function feature of the total DNA-binding site of the helicases.[31-33] However, very little is known about the role of the strong and weak DNA-binding subsites in the mechanism of the DNA entry into the cross channel of a hexameric helicase.

Functional and structural homology between the RepA hexamer and the DnaB helicase hexamer makes the RepA protein an excellent model for comparative studies of general aspects of interactions between the hexameric replicative helicase and the DNA.[8,9,12-14,21,28] The role of conformational changes of the protein accompanying the association with the ssDNA should be much more pronounced, due to the small size of the cross channel and the extreme stability of the RepA hexamer, than in the case of less stable enzymes. Moreover, quantitative kinetic mechanism of interactions with the ssDNA is currently known only for two hexameric helicases, making any mechanistic generalization very difficult.[29,30,34] The paramount role of RepA helicase in the RSF1010 plasmid replication indicates the presence of some specific mechanism of replicative helicase activities, which is not yet recognized. Furthermore, the fact that the RepA helicase plays an essential role in replication of the RSF1010 plasmid, which confers resistance to antibiotics, gives an opportunity to address the molecular aspects of such resistance.[8-11,21,28]

In this communication, we describe quantitative analyses of the kinetic mechanism of the ssDNA entry into the cross channel of the RepA helicase. Extreme stability of the RepA hexamer precludes any disintegration of its structure prior to the association with the nucleic acid, and the enzyme exists in a single conformation preceding the association reaction. Moreover, the helicase possesses a DNA-binding site located outside its cross channel, which initially binds the DNA. The reaction steps comprise binding steps and large conformational transitions of the enzyme, including local opening of the hexameric structure with different thermodynamic characteristics. The entry of the nucleic acid into the cross channel is initiated from the 5′ end of the bound DNA. Furthermore, in equilibrium, the RepA hexamer–ssDNA complex exists in a mixture of partially open states.

Results

Dynamics of the ssDNA binding to the total DNA-binding site of the RepA helicase

Because the total DNA-binding site of the RepA hexamer occludes 19±1 nucleotides, the helicase binds only a single molecule of the ssDNA 20-mer and the oligomer encompasses the entire total binding site of the enzyme.[12] By the same token, only a single RepA hexamer binds to the ssDNA oligomers up to 37 nucleotides in length, engaging the entire DNA-binding site. To examine the mechanism of the DNA association with the total DNA-binding site of the RepA helicase, we selected a series of ssDNA oligomers, containing 20, 25, and 30 nucleotides, which can accept only a single hexamer molecule (see below). Although binding of the ssDNA to the RepA helicase is not accompanied by any significant change of the protein fluorescence, we previously found that association of the oligomers, labeled at the 5′ end with the fluorescent marker fluorescein, is accompanied by a large quenching of the emission intensity of the marker, providing an excellent signal to monitor the complex kinetics of the helicase–ssDNA interactions.[12] Because fluorescein is introduced through the phosphoramidate chemistry (Materials and Methods), the marker constitutes an additional residue in the selected nucleic acids. Therefore, the ssDNA oligomers are further referred as 21-, 26-, and 31-mers. Thermodynamic studies have showed that the presence of the marker does affect the energetics of the enzyme–ssDNA interactions.[12]

All stopped-flow experiments discussed in this work have been performed under pseudo-first-order conditions with respect to the protein, by mixing the ssDNA oligomer with a

large excess of the RepA helicase.[29,30,35-38] The stopped-flow kinetic trace of the 5′-Fl-dT$(pT)_{19}$ fluorescence, after mixing 5×10^{-9} M (oligomer) with 5×10^{-7} M RepA helicase (hexamer) (final concentrations) in buffer T5 (pH 7.6, 10 °C), containing 0.5 mM β,γ-imidoadenosine-5′-triphosphate (AMP-PNP), is shown in Fig. 2. The observed signal is the total fluorescence emission of the sample, which eliminates possible artifacts, resulting from the changes of the fluorescence anisotropy of the sample (Materials and Methods).[37,38] The curve is shown in two time bases, 5 and 1500 s. The kinetic relaxation process is complex. A fast step is followed by a much slower intensity decay, as the system approaches equilibrium. The continuous line in Fig. 2 is a nonlinear least-squares fit of the experimental curve using a three-exponential function (Materials and Methods).[29,30,35-38] As indicated by the included deviations of the experimental curve from the fit, the three-exponential function provides an adequate description of the experimentally observed kinetics. However, the same process monitored by the fluorescence anisotropy clearly indicates the presence of an additional fast step (see below), although a higher number of exponents does not significantly improve the statistics of the total emission intensity fit (data not shown). Therefore, the association of the ssDNA 20-mer with the total DNA-binding site of the RepA helicase is a process, which includes at least four steps.[29,30,35-40]

The dependence of the reciprocal relaxation times, $1/\tau_1$,$1/\tau_2$, and $1/\tau_3$, characterizing the observed kinetic steps, as a function of the total RepA concentration, $[RepA]_T$, is shown in Fig. 3a–c. The largest reciprocal relaxation time, $1/\tau_1$, shows little dependence upon $[RepA]_T$, indicating that it characterizes an intramolecular step.[29,30,35-40] Moreover, the fact that anisotropy data provide strong evidence for the presence of an additional fast step, $1/\tau_1$, characterizes an intramolecular transition (see below). A similar behavior is observed for $1/\tau_2$, which has ~3 orders of magnitude lower values than $1/\tau_1$, indicating a much slower transition of the complex (Fig. 3b). Also, $1/\tau_3$ does not show any pronounced dependence upon $[RepA]_T$ (Fig. 3c). Thus, the simplest minimum mechanism that can account for the observed dependence of the relaxation times upon the RepA concentration is a four-step, sequential binding process, in which the bimolecular association is followed by three isomerization steps, as described in Eq. (1)

$$\begin{aligned} &\mathrm{RepA}+\mathrm{ssDNA} \underset{k_{-1}}{\overset{k_1}{\longleftrightarrow}} (\mathrm{H}-\mathrm{ssDNA})_1 \underset{k_{-2}}{\overset{k_2}{\longleftrightarrow}} (\mathrm{H}-\mathrm{ssDNA})_2 \underset{k_{-3}}{\overset{k_3}{\longleftrightarrow}} \\ &(\mathrm{H}-\mathrm{ssDNA})_3 \underset{k_{-4}}{\overset{k_4}{\longleftrightarrow}} (\mathrm{H}-\mathrm{ssDNA})_4 \end{aligned} \tag{1}$$

In the numerical analyses, to extract the rate constants from the relaxation time data in Fig. 3a–c, we utilize the fact that the value of the overall binding constant, $K_{21} = (3.1 \pm 0.4) \times 10^6$ $M^{-}1$, has previously been independently obtained in the same solution conditions by the equilibrium fluorescence titration method.[12] The overall binding constant K_{21} is related to the partial equilibrium steps by Eq. (2), as

$$K_{21}=K_1\,(1+K_2+K_2K_3+K_2K_3K_4) \tag{2}$$

where the partial equilibrium constants for each step of the reaction, described in Eq. (1), are $K_1 = k_1/k_{-1}$, $K_2 = k_2/k_{-2}$, $K_3 = k_3/k_{-3}$, and $K_4 = k_4/k_{-4}$. Equation (2) reduces the number of fitting parameters by 1 (see below).

The dependence of the individual amplitudes A_1, A_2, and A_3 of all three observed relaxation processes upon the total concentration of RepA hexamer is shown in Fig. 3d. The individual amplitudes are normalized; that is, expressed as fractions of the total amplitude, $A_i/\sum A_i$. At a low enzyme concentration, the contribution of amplitudes A_1 and A_3 of the fastest and

slowest relaxation steps, respectively, dominates the total observed amplitude A_T. The amplitude A_1 steadily increases with the increase of the protein concentration, while A_3 strongly decreases with the increase of $[RepA]_T$. The values of the amplitude of the second step, A_2, remains low and decreases with $[RepA]_T$. Such behavior of the individual amplitudes is in complete agreement with the proposed kinetic mechanism [Eq. (1)] based on the behavior of the relaxation times and anisotropy data (see below).[29,30,35-39]

Having determined individual amplitudes, one can address the molar fluorescence intensities characterizing each intermediate of the reaction, using the matrix projection operator approach (Materials and Methods).[29,30,35-39] In this case, we use the maximum fractional quenching of the nucleic acid fluorescence, $\Delta F_{max} \approx 0.2$, obtained in independent equilibrium titrations.[12,39] The values of ΔF_{max} can be analytically expressed as

$$\Delta F_{max} = \frac{K_1 \Delta F_1 + K_1 K_2 \Delta F_2 + K_1 K_2 K_3 \Delta F_3 + K_1 K_2 K_3 K_4 \Delta F_4}{1 + K_1 K_2 + K_1 K_2 K_3 + K_1 K_2 K_3 K_4} \quad (3)$$

where ΔF_1, ΔF_2, ΔF_3, and ΔF_4 are fractional fluorescence intensities of the corresponding intermediates in the association reaction of the 21-mer with the RepA hexamer, relative to the fluorescence of the free nucleic acid, F_0; that is, $\Delta F_i = (F_i - F_0)/F_0$. The value of F_0 can be taken as 1. Equation (3) furnishes an additional relationship among the fluorescence parameters, with the value of ΔF_{max} playing the role of a scaling factor.[29,30,35-39]

The continuous lines in Fig. 3a–d are nonlinear least-squares fits of the experimentally determined relaxation times and fractional individual amplitudes of the reaction, defined in Eq. (1), using a single set of binding and spectroscopic parameters and using the matrix projection operator methods together with Eqs. (2) and (3) (Materials and Methods).[29,30,35-39] First, the numerical analysis was performed by nonlinear least-squares fitting of the individual relaxation times and then simultaneous fitting of all three relaxation times. Subsequently, nonlinear least-squares fitting was performed with the individual amplitudes, using the rate constants obtained from the relaxation time analysis or allowing the rate constants to float between +10% and −10% of the determined values. Finally, global fitting, with the simultaneous analysis of all relaxation times and individual amplitudes, refines the obtained parameters. Analogous stopped-flow and numerical analyses have been performed for all examined ssDNA oligomers, 5′-Fl-dT(pT)$_{19}$, 5′-Fl-dT(pT)$_{24}$, and 5′-Fl-dT(pT)$_{29}$, which engage the total DNA-binding site of the RepA helicase.[12] The obtained partial equilibrium constants, rate constants, and spectroscopic parameters characterizing the intermediates of the reaction for all examined oligomers are included in Table 1.

The values of the partial equilibrium constant, K_1, which describes the formation of the first intermediate $(H\text{-ssDNA})_1$ in Eq. (1), changes from ~1.5×10^5 $M^{-}1$ for the 21-mer to ~5×10^4 M^{-1} for the 31-mer. A statistical factor of the form $N-n+1$, where N is the length of the oligomer and n is the site size of the complex (in our case, n = 19 for the total DNA-binding site of the RepA hexamer), is expected for the large ligand binding to a homogeneous nucleic acid lattice.[41-44] The data indicate that there is no statistical factor involved in the formation of the first intermediate for the 21-, 25-, and 31-mer. A similar lack of the statistical effect in the RepA hexamer binding to the corresponding ssDNA oligomers has been previously observed for the overall equilibrium constant, K_N, in equilibrium studies[12] (see Discussion). Nevertheless, the formation of the first intermediate has a predominant contribution to the free energy of ssDNA binding. At 10 °C, the next three steps of the reaction increase the overall affinity. Moreover, the partial equilibrium constants have very similar values for all examined oligomers. The value of K_2, which characterizes the transition $(H\text{-ssDNA})_1 \leftrightarrow (H\text{-ssDNA})_2$, is in the range of ~2.3–2.5. The values of K_3, which

describes the transition $(H\text{-}ssDNA)_2 \leftrightarrow (H\text{-}ssDNA)_3$, is in the range of ~2.5–3.8, while the final step, $(H\text{-}ssDNA)_3 \leftrightarrow (H\text{-}ssDNA)_4$, is described by the partial equilibrium constant, K_4, with the values in the range of ~1.9–4.0 (Table 1). However, in spite of similar partial equilibrium constants, the dynamics of the second step, $(H\text{-}ssDNA)_1 \leftrightarrow (H\text{-}ssDNA)_2$, of the reaction is very different from the dynamics of the remaining two steps. The values of the forward and backward rate constants, k_2 and k_{-2}, are ~3 orders of magnitude larger than the values of k_3, k_{-3}, k_4,and k_{-4} (Table 1). These data provide the first indication that processes of a different nature are involved in the observed relaxation steps (see Discussion).

The difference between the first and the remaining intermediates is clearly seen in the corresponding changes of the fluorescence emission of the nucleic acid, originating from the fluorescein marker located at the 5′ end of the examined ssDNA oligomers (Table 1). The results indicate that there is no fluorescence change, as compared to the free ssDNA, in the first binding step, that is, in the formation of $(H\text{-}ssDNA)_1$, indicating that in the first intermediate, the marker is in an environment similar to the bulk solution.[45,46] This is very different from the large fluorescence changes observed for the first intermediate in the complex formation between the *E. coli* DnaB hexamer and the etheno derivative of the ssDNA 20-mer, $d\varepsilon A(p\varepsilon A)_{19}$ (see Discussion).[29] Nevertheless, the subsequent conformational transition, $(H\text{-}ssDNA)_1 \leftrightarrow (H\text{-}ssDNA)_2$, induces significant quenching of the fluorescein emission. This is particularly pronounced for the two longer oligomers, 5′-Fl-$dT(pT)_{24}$ and 5′-Fl-$dT(pT)_{29}$,with $F_2 \approx 0.2$, as compared to the free nucleic acid, indicating that the marker is placed in a very different environment in $(H\text{-}ssDNA)_2$ than in $(H\text{-}ssDNA)_1$.[45,46] Emission intensity of the marker is also quenched in the intermediates $(H\text{-}ssDNA)_3$ and $(H\text{-}ssDNA)_4$ for all examined ssDNAs, although to a lesser extent than in $(H\text{-}ssDNA)_2$.

Dynamics of the ssDNA binding to the strong DNA-binding subsite of the RepA hexamer

As mentioned above, the total ssDNA-binding site of the RepA helicase is composed of two DNA-binding subsites, differing by at least 2 orders of magnitude in their intrinsic affinities for the nucleic acid.[12] The strong DNA-binding subsite is located in the vicinity of the small domain of each protomer of the RepA hexamer (Fig. 1) and can accept the ssDNA fragment up to 11 nucleotides.[12] Therefore, the mechanism of the DNA binding to the RepA hexamer has been addressed using a series of ssDNA oligomers, 5′-Fl-$dT(pT)_7$,5′-Fl-$dT(pT)_8$, and 5′-Fl-$dT(pT)_9$, which exclusively bind to the strong subsite.[12]

The reciprocal relaxation times $1/\tau_1$, $1/\tau_2$, and $1/\tau_3$ characterizing the observed kinetic steps in the association reaction of the 10-mer, 5′-Fl-$dT(pT)_8$, with the RepA hexamer, in buffer T5 (pH 7.6, 10 °C), containing 0.5 mM AMP-PNP, as a function of the total RepA concentration, are shown in Fig. 4a–c. The values of the largest relaxation time, $1/\tau_1$, are significantly larger than those observed for the 21-, 26-, and 31-mers, indicating that the first relaxation step is faster than the corresponding process observed for the oligomers that can engage the total DNA-binding site (see below). Moreover, $1/\tau_1$ shows only a little dependence upon $[RepA]_T$, an indication that it characterizes an intramolecular step (see above).[29,30,35-40] As discussed above, the anisotropy data provide strong evidence of the presence of an additional fast step, corroborating the conclusion that $1/\tau_1$ characterizes an intramolecular transition. The behavior and the values of $1/\tau_2$ and $1/\tau_3$ are very similar to the behavior and values of the corresponding parameters observed for the 21-, 26-, and 31-mers (Fig. 3a–c). Thus, the minimum mechanism of the 10-mer binding to the strong DNA-binding subsite of the RepA hexamer, which can account for all kinetic data, is a four-step, sequential binding process, as described in Eq. (1).

The dependence of the normalized individual amplitudes, A_1, A_2, and A_3, of the observed relaxation processes, in the binding of the 10-mer to the RepA hexamer, upon the total

concentration of RepA hexamer concentration, is shown in Fig. 4d. The behavior of the amplitudes is different from the behavior observed in the case of the 21-mer (Fig. 3d), providing the first indication of different partial equilibria among the observed intermediates, as compared to the oligomer, which encompasses the total DNA-binding site.[29,30,35-40] At low enzyme concentrations, only amplitude A_3 of the slowest relaxation step has a dominant contribution to the total observed amplitude, A_T. The amplitude of the fastest observed process, A_1, has the lowest value of all observed amplitudes over the entire range of the examined protein concentrations and only gradually increases with increasing $[RepA]_T$. On the other hand, the amplitude of the second step, A_2, is much larger than that observed for the 21-mer (Fig. 3d) and, at high $[RepA]_T$, dominates the total amplitude of the reaction. Nevertheless, the observed behavior of the individual amplitudes is in complete agreement with the proposed kinetic mechanism [Eq. (1)].[29,30,35-39]

The strategy of the numerical analysis of the data was the same as described above for the 21-mer (see above). The continuous lines in Fig. 4a–d are nonlinear least-squares fits of the experimentally determined relaxation times and normalized individual amplitudes of the reaction, defined in Eq. (1), using a single set of kinetic and spectroscopic parameters. Analogous stopped-flow and numerical analyses have been carried out for the 9- and the 11-mer, 5′-Fl-dT$(pT)_7$ and 5′-Fl-dT$(pT)_9$, which also exclusively engage in interactions with the strong DNA-binding subsite of the RepA helicase.[12] The obtained partial equilibrium constants, rate constants, and spectroscopic parameters characterizing the intermediates of the reaction for all examined oligomers are included in Table 2.

Unlike the case of the 21-, 26-, and 31-mers, the values of the partial equilibrium constant, K_1, which characterizes the formation of the first intermediate, $(H\text{-}ssDNA)_1$, clearly increase with the length of the oligomer from ~5×10^4 to ~2×10^5 M^{-1} obtained for the 9- and the 11-mer, respectively. Thus, there is a statistical factor, $N-n+1$, involved in the formation of the first intermediate, where $n = 8$ for the strong DNA-binding subsite of the RepA hexamer (see above).[41-44] Within experimental accuracy, the obtained statistical factor is similar to the same factor determined in the equilibrium binding of the corresponding ssDNA oligomers to the RepA hexamer[12] (see Discussion). Similar to the 21-, 26-, and 31-mers, the formation of the first intermediate has a predominant contribution to the free energy of the ssDNA binding to the strong DNA-binding subsite. At 10 °C, the values of K_2 characterizing the transition $(H\text{-}ssDNA)_1 \leftrightarrow (H\text{-}ssDNA)_2$ is in the range of ~0.7–1.4, that is, also similar to the values of the same parameter observed for the longer oligomers (Table 1). However, the values of K_3, which characterizes the transition $(H\text{-}ssDNA)_2 \leftrightarrow (H\text{-}ssDNA)_3$, is in the range of ~11.5–16. Thus, the formation of the intermediate $(H\text{-}ssDNA)_3$ is significantly more energetically favorable in the case of the oligomers that exclusively bind to the strong DNA-binding subsite than that observed for the oligomers that engage the total DNA-binding site. On the other hand, the partial equilibrium constant, K_4, is in the range of ~0.8–1.7, which is lower than those observed for the 21-, 26-, and 31-mers (Tables 1 and 2) (see Discussion).

Similar to the oligomers that engage the total DNA-binding site, the dynamics of the transition $(H\text{-}ssDNA)_1 \leftrightarrow (H\text{-}ssDNA)_2$ is approximately 2–3 orders of magnitude faster than the dynamics of the remaining two steps of the reaction (Tables 2). As mentioned above, these data indicate that processes of different natures are involved in the observed relaxation steps (see Discussion). Nevertheless, with the exception of the 11-mer, 5′-Fl-dT $(pT)_9$, the forward and backward rate constants, k_2 and k_{-2}, are ~1 order of magnitude larger than the values of the same parameters obtained for the oligomers that engage the total DNA-binding site. Moreover, k_2 and k_{-2} decrease with the length of the oligomer and, in the case of the 11-mer, approach the values of the corresponding parameters observed for the 21-, 26-, and 31-mers (Table 2). The forward rate constant, k_3, characterizing the transition (H-

ssDNA)$_2$↔(H-ssDNA)$_3$ is similar to the corresponding parameter observed for the 21-, 26-, and 31-mers. However, the values of the backward rate constant, k_{-3}, are generally lower than the values of k_{-3} determined for the longer oligomers (see Discussion). In other words, it is more difficult for the shorter oligomers to return to the (H-ssDNA)$_2$ intermediate, once they entered (H-ssDNA)$_3$ than for the longer nucleic acids. In general, the dynamics of the transition (H-ssDNA)$_3$↔(H-ssDNA)$_4$ is also different from the behavior of the longer oligomers (Tables 1 and 2). The forward rate constant, k_4, is lower and the backward rate constant, k_{-4}, is higher for the oligomers that exclusively bind to the strong DNA-binding subsite than that for the oligomers that engage the total DNA-binding site.

Amplitude analysis indicates that the behavior of the fluorescence emission of the fluorescein marker is analogous, although not the same, to the behavior observed for the longer oligomers (Tables 1 and 2). There is no fluorescence change, as compared to the free nucleic acid, in the binding step (Table 2). Thus, in the intermediate (H-ssDNA)$_1$, the marker seems to be in an environment similar to the bulk solution, independent of the length of the bound ssDNA oligomer (Tables 1 and 2). The subsequent conformational transition (H-ssDNA)$_1$↔(H-ssDNA)$_2$ induces significant quenching of the fluorescein emission of the bound DNA. Nevertheless, there is no clear trend in the observed quenching of the emission intensities with the changing length of the bound oligomer, as observed for the oligomers that engage the total DNA-binding site (Table 1), with the highest quenching observed for the 10-mer, 5′-Fl-dT(pT)$_8$. With the exception of the 10-mer, transition to the intermediate (H-ssDNA)$_3$ does not induce further changes in the emission intensity of the marker, which remains similar to the emission observed for (H-ssDNA)$_2$, while the transition to subsequent intermediate (H-ssDNA)$_4$ is accompanied by significant additional quenching only in the case of the 11-mer, 5′-Fl-dT(pT)$_9$ (see Discussion).

Temperature effect on the ssDNA-binding dynamics to the total DNA-binding site and to the strong DNA-binding subsite of the RepA hexamer

In order to further address the nature of different intermediates in the RepA hexamer binding to the ssDNA, we examined the temperature effect on the dynamics of the reaction. The experiments have been performed using the ssDNA 21- and 31-mer, which engage the total DNA-binding site in interactions, and with the 10- and 11-mer, which exclusively bind to the strong DNA-binding subsite.[12] The stopped-flow studies were carried out at two different temperatures, analogously, as described above (data not shown). The obtained kinetic and spectroscopic parameters for all examined complexes are included in Tables 1 and 2. In general, the temperature increase from 10 to 20 °C does not affect the major features of the observed kinetic mechanism, which, at both temperatures, is the four-step sequential process, described in Eq. (1). However, the effect of the temperature on internal equilibria differs among the reaction intermediates and is different for the total DNA-binding site, as compared to the strong DNA-binding subsite.

In the case of 21- and 31-mer, the partial equilibrium constant K_1, characterizing the binding step RepA hexamer+ssDNA↔(H-ssDNA)$_1$, is decreased, by a factor of ~2–3, with the temperature increase. This step is too fast to address its dynamics in the stopped-flow experiment. The partial equilibrium constant K_2, characterizing the transition (H-ssDNA)$_1$↔(H-ssDNA)$_2$, is increased by a similar factor at a higher temperature, primarily due to the increased forward rate constant, k_2, while k_{-2} remains only slightly affected by temperature (Table 1). Analogously, the value of K_3, which describes the transition (H-ssDNA)$_2$↔(H-ssDNA)$_3$, is higher at a higher temperature. However, this occurs primarily due to the decrease of the backward rate constant, k_{-3}, while k_3 remains slightly affected. On the other hand, the value of K_4, characterizing the final transition (H-ssDNA)$_3$↔(H-ssDNA)$_4$, decreases with an increase in temperature, by a factor of ~2, mainly due to the decrease of the forward rate constant k_4.

In the case of the ssDNA oligomers that bind to the strong DNA-binding subsite of the RepA hexamer, both partial equilibrium constants K_1 and K_2, characterizing the binding step RepA hexamer+ssDNA↔(H-ssDNA)$_1$ and the transition (H-ssDNA)$_1$↔(H-ssDNA)$_2$, decrease at higher temperature. However, unlike the behavior of the 21- and 31-mer, there is a very strong effect of the temperature on both k_2 and k_{-2}, with k_2 increasing by more than 1 order of magnitude at the elevated temperature (Table 2). As a result, the transition (H-ssDNA)$_1$↔(H-ssDNA)$_2$ becomes ~1 order of magnitude faster for the 10- and 11-mer, which engage the strong DNA-binding subsite, than that observed for the ssDNA oligomers that engage the total DNA-binding site (see Discussion). Instead of an increase, as observed for the 21- and 31-mer, there is a decrease in the value of K_3, with the temperature for the 10- and 11-mer, due to the significant increase in the backward rate constant k_{-3}. Nevertheless, similar to the 21- and 31-mer, the partial equilibrium constant K_4 decreases at higher temperature, predominantly due to the increase in the backward rate constant k_{-4}, while k_4 remains only slightly affected by the temperature (Table 2).

The temperature dependence of the partial equilibrium constant K_i for each ith transition in the process of the RepA hexamer binding to the ssDNA is described by van't Hoff's equation[47]

$$\frac{\partial \ln K_i}{\partial \left(\frac{1}{T}\right)} = -\frac{\Delta H_i}{R}\left(\frac{1}{T} - \frac{1}{T_R}\right) \quad (4)$$

where T_R is the reference temperature, taken as the lowest experimentally studied temperature, that is, 10 °C, and ΔH_i is the enthalpy change accompanying the ith transition. The obtained values of the thermodynamic function, ΔH_i and ΔS_i, characterizing the partial equilibria among the intermediates of the ssDNA binding to the total DNA-binding site and the strong DNA-binding subsite of the RepA hexamer, for all examined oligomers, are included in Table 3. The errors in the determined parameters are inherently large. Nevertheless, the observed differences are larger than the errors and provide an important insight about the nature of the observed transitions.

The first step, that is, binding of the ssDNA to the total DNA-binding site and to the strong DNA-binding subsite, is characterized by negative enthalpy and entropy changes, suggesting a similar nature of both binding processes (see Discussion). In the next transition, (H-ssDNA)$_1$↔(H-ssDNA)$_2$, both ΔH_2 and ΔS_2 are positive, suggesting that a process of a different nature than the first binding step is observed in the interactions with the total DNA-binding site, as well as in interactions with the strong DNA-binding subsite (see Discussion). On the other hand, changes of the thermodynamic functions in the third transition, (H-ssDNA)$_2$↔(H-ssDNA)$_3$, differ for the association of the nucleic acid with the total binding site, as compared to the strong binding subsite (Table 3). The values of ΔH_3 and ΔS_3 are negative for the 10- and 11-mer, while the corresponding parameters are positive for the 21- and 31-mer, suggesting that the nature of the transition is different for the total DNA-binding site, as compared to the strong binding subsite. In the final transition, (H-ssDNA)$_3$↔(H-ssDNA)$_4$, the values of ΔH_4 and ΔS_4 are negative for both the total binding site and the strong binding subsite, suggesting a similar process leading to the formation of the intermediate (H-ssDNA)$_4$ (see Discussion).

The fractional distributions of the intermediates of the RepA hexamer binding to the ssDNA

The fractional distributions of the ssDNA intermediates for the ssDNA oligomer, which encompasses the total DNA-binding site of the RepA hexamer, at two different temperatures

are shown in Fig. 5a and b. The plots are presented in semilogarithmic scale and were generated using the rate constants for the 21-mer (Table 1). The concentrations of the intermediates are normalized as molar fractions of the total concentration of the DNA oligomer. At the selected protein concentration, the nucleic acid is predominantly saturated with the enzyme. At 10 °C, the first intermediate, $(H\text{-}ssDNA)_1$, significantly contributes to the total population of the nucleic acid states over a large time span of the reaction. However, when the system reaches equilibrium, the $(H\text{-}ssDNA)_1$ intermediate constitutes only ~2% of the total DNA population. At 20 °C, the fractional contribution of $(H\text{-}ssDNA)_1$ strongly diminishes and becomes negligible at equilibrium (Fig. 5b). The fractional contribution of the second intermediate, $(H\text{-}ssDNA)_2$, is much less dependent upon the temperature than the first intermediate, and it has a significant contribution, ~53–60%, to the total population over the time course of the reaction. At equilibrium, $(H\text{-}ssDNA)_2$ constitutes ~8–11% of the total population of the nucleic acid (Fig. 5a and b). Both the third and the fourth intermediate, $(H\text{-}ssDNA)_3$ and $(H\text{-}ssDNA)_4$, dominate the population of the bound nucleic acid at equilibrium. However, their mutual proportions change with temperature. At 10 °C, the fourth intermediate, $(H\text{-}ssDNA)_4$, is in slight excess, while at the higher temperature, the fractional contribution of $(H\text{-}ssDNA)_3$ is significantly larger than that of $(H\text{-}ssDNA)_4$ (Fig. 5b) (see Discussion).

The fractional distributions of the intermediates for the 11-mer, which exclusively binds to the strong DNA-binding subsite, are shown in Fig. 5c and d, for the examined temperatures. The first intermediate, $(H\text{-}ssDNA)_1$, has a larger contribution to the total population of the bound nucleic acid, at both 10 and 20 °C, than in the case of the 21-mer. Nevertheless, its fractional contribution becomes very low, ~2%, at equilibrium. On the other hand, the second intermediate, $(H\text{-}ssDNA)_2$, constitutes a much lower fraction of the total population of the nucleic acid than in the case of the 21-mer. Moreover, it only has a 2–5% fractional contribution to the total nucleic acid population at equilibrium. Nevertheless, similar to the 21-mer, the fractional contribution of $(H\text{-}ssDNA)_2$ shows a modest dependence upon the temperature. Similar to the 21-mer, both the third and the fourth intermediate, $(H\text{-}ssDNA)_3$ and $(H\text{-}ssDNA)_4$, dominate the population of the bound nucleic acid at equilibrium. However, the third intermediate, $(H\text{-}ssDNA)_3$, is at a significantly larger excess, ~50%, at both examined temperatures than the final intermediate, $(H\text{-}ssDNA)_4$, whose fractional contribution diminishes from ~31% to ~20% as the temperature increases (see Discussion).

Global conformation of the RepA hexamer–ssDNA complex in solution: Analytical sedimentation velocity studies

The analytical sedimentation technique provides direct information about the hydrodynamic properties of a macromolecule.[15,21,48-53] In turn, the hydrodynamic properties reflect global conformational states of the macromolecule in solution. We utilize the fact that the sedimentation coefficients of the ssDNA 21- and 11-mer, 5′-Fl-$dT(pT)_{19}$ and 5′-Fl-$dT(pT)_9$ (~1.3 and ~1.5 S, respectively), which contain fluorescein at their 5′ ends, are much smaller than the sedimentation coefficient of the binary complex RepA hexamer–AMP-PNP (~8.5 S).[21] Therefore, the sedimentation of the nucleic acid in the complex can be exclusively monitored at the fluorescein absorption band (495 nm), without any interference from the free protein and nucleotide cofactor absorbance.[15,16,27,31,54,55]

Sedimentation velocity profiles of the ssDNA 11-mer, 5′-Fl-$dT(pT)_9$, alone in buffer T5 (pH 7.6, 10 °C), containing 0.5 mM AMP-PNP, are shown in Fig. 6a. The profiles have been recorded at a rotational speed of 35,000 rpm. The total nucleic acid concentration is 5×10^{-6} M (oligomer). It is evident that, in the applied rotational speed, the sedimentation boundary of the nucleic acid moves very slowly from the meniscus. The situation is different in the presence of the RepA hexamer. Sedimentation velocity profiles of the ssDNA 11-mer, 5′-Fl-$dT(pT)_9$, in the presence of the RepA hexamer in buffer T5 (pH 7.6, 10 °C), containing 0.5

mM AMP-PNP, are shown in Fig. 6b. Analogous sedimentation velocity profiles for the 21-mer, 5′-Fl-dT(pT)$_{19}$, are shown in Fig. 6c. In both sets of experiments, the profiles have been recorded at the fluorescein absorption band (495 nm). The total DNA and protein concentrations are 5×10^{-6} M (oligomer) and 8×10^{-6} M (hexamer), respectively. At the selected RepA concentration, the enzyme completely saturates the ssDNA oligomers.[12] Inspection of the profiles in Fig. 6b and c shows that there is an apparent single moving sedimentation boundary, indicating the presence of a single molecular species, for both the 11- and 21-mer.[15,16,27,31,54-56] Independent sedimentation equilibrium experiments confirm the presence of a single species with molecular masses of 187,000 ± 9000 and 185,000 ± 9000 Da, respectively (data not shown). To obtain the apparent average sedimentation coefficient, $s_{20,w}$, of both tertiary complexes, RepA–ssDNA–AMP-PNP, we analyzed the sedimentation velocity scans using the time-derivative approach, which provides $s_{20,w}$ = 9.8±0.1 S and $s_{20,w}$ = 10.0± 0.1 S for the complex with the 11- and 21-mer, respectively.[50,51] An example of the nonlinear least-squares fit for the RepA-5′-Fl-dT(pT)$_{19}$ complex is shown in Fig. 6d.

In analogous solution conditions and in the presence of 0.5 mM AMP-PNP, the apparent average sedimentation coefficient ($s_{20,w}$) of the binary complex RepA hexamer–AMP-PNP is 8.5±0.1 S; that is, the data show that the tertiary complex has a dramatically increased sedimentation coefficient, as compared to the binary complex.[21] The molecular masses of the 21-and 11-mer are ~6700 and ~3500 Da, respectively. Thus, the ssDNA oligomers constitute ~3.5% and ~2% of the mass of the corresponding complex, respectively. The observed large increase of the apparent average sedimentation coefficient of the RepA hexamer in the tertiary complex with both ssDNA oligomers cannot be explained by the increased molecular weight of both complexes. Moreover, the 21-mer, twice as large, induces a very similar increase of the sedimentation coefficient, as observed for the 11-mer (Fig. 6b and c). Because only a single molecular species is present in both samples (see above), the observed large increase in the apparent average sedimentation coefficient of the tertiary complex, with little dependence upon the length of the bound ssDNA oligomer, must result from the large global conformational changes of the RepA hexamer, when the enzyme–AMP-PNP complex is associated with the nucleic acid (see Discussion).

Stopped-flow, fluorescence anisotropy studies of the ssDNA binding to the total DNA-binding site of the RepA hexamer: Experiments with the ssDNA oligomers labeled at the 5′ or 3′ end of the nucleic acid

In the kinetic experiments described above, the dynamics of the nucleic acid association with the RepA hexamer was followed by monitoring the total emission of the sample, $F(t)$ (Materials and Methods). While fluorescence intensity provides information about the physical environment surrounding the fluorophore, time dependence of the fluorescence anisotropy, in stopped-flow experiments, provides information about the mobility of the fluorescing ligand, during the fluorescence lifetime of the individual intermediates.[37,38,57] Moreover, anisotropy data may also add additional light on the mechanism of the reaction (see below).[57] Because the lifetime of the fluorescein is ~4 ns, that is, it is orders of magnitude shorter than the lifetime of any intermediate formed in the kinetic reaction, stopped-flow fluorescence anisotropy studies provide the values of the steady-state anisotropy of the nucleic acid molecule in each intermediate.

Unlike the total emission, stopped-flow kinetic traces, recorded using the fluorescence anisotropy, are not a simple sum of exponential functions, even under pseudo-first-order conditions.[38,57] The time course of the fluorescence anisotropy of the sample is defined as

$$r(t) = \frac{I_{VV}(t) - I_{VH}(t)}{I_{VV}(t) + 2GI_{VH}(t)} \tag{5}$$

which can be written as

$$r(t) = \sum_{i=1}^{n} f_i(t)\ r_i \tag{6}$$

where $f_i(t)$ is the time-dependent fractional contribution of ith fluorescing intermediate of the reaction to the total emission of the sample and r_i is its corresponding steady-state fluorescence anisotropy. For the specific mechanism of the ssDNA binding to the RepA hexamer, defined in Eq. (1), Eq. (6) takes form, as

$$r(t) = f_0(t)\, r_{D0} + f_1(t)\, r_{D1} + f_2(t)\, r_{D2} + f_3(t)\, r_{D3} + f_4(t)\, r_{D4} \tag{7}$$

where r_{D1}, r_{D2}, r_{D3}, and r_{D4} are steady-state anisotropies of the free nucleic acid in (H-ssDNA)$_1$, (H-ssDNA)$_2$, (H-ssDNA)$_3$, and (H-ssDNA)$_4$ intermediates. Using the expansion of the original coefficient matrix of the reaction, **M**, by matrix projection operators (Materials and Methods), we define the time course of the fluorescence anisotropy in Eq. (7) as

$$r(t) = \frac{\begin{pmatrix} F_0 r_{D0} & F_1 r_{D1} & F_2 r_{D2} & F_3 r_{D3} & F_4 r_{D4} \end{pmatrix} \begin{pmatrix} P_{01} & P_{11} & P_{21} & P_{31} & P_{41} \\ P_{02} & P_{12} & P_{22} & P_{32} & P_{42} \\ P_{03} & P_{13} & P_{23} & P_{33} & P_{43} \\ P_{04} & P_{14} & P_{24} & P_{34} & P_{44} \\ P_{05} & P_{15} & P_{25} & P_{35} & P_{45} \end{pmatrix} \begin{pmatrix} 1 \\ \exp(\lambda_1 t) \\ \exp(\lambda_2 t) \\ \exp(\lambda_3 t) \\ \exp(\lambda_4 t) \end{pmatrix}}{F(t) = \begin{pmatrix} F_0 & F_1 & F_2 & F_3 & F_4 \end{pmatrix} \begin{pmatrix} P_{01} & P_{11} & P_{21} & P_{31} & P_{41} \\ P_{02} & P_{12} & P_{22} & P_{32} & P_{42} \\ P_{03} & P_{13} & P_{23} & P_{33} & P_{43} \\ P_{04} & P_{14} & P_{24} & P_{34} & P_{44} \\ P_{05} & P_{15} & P_{25} & P_{35} & P_{45} \end{pmatrix} \begin{pmatrix} 1 \\ \exp(\lambda_1 t) \\ \exp(\lambda_2 t) \\ \exp(\lambda_3 t) \\ \exp(\lambda_4 t) \end{pmatrix}} \tag{8}$$

The generalization of the above expression to any kinetic mechanism is straightforward.[38]

In the first set of experiments, we addressed the dynamics of the anisotropy changes accompanying the binding of the ssDNA 21-mer, labeled at the 5′ end with the fluorescein, 5′-Fl-dT(pT)$_{19}$. The stopped-flow kinetic trace of the fluorescence anisotropy of 5′-Fl-dT(pT)$_{19}$, after mixing the nucleic acid with the RepA hexamer in buffer T5 (pH 7.6, 20 °C), containing 0.5 mM AMP-PNP, is shown in Fig. 7a. The final concentrations of the DNA and the enzyme are 5×10^{-9} and 1×10^{-6} M, respectively. Because of the high noise in the shorter time range (Fig. 2), the trace was recorded in the range from 1 to 2000 s, in the "oversampling" mode (Materials and Methods). The anisotropy rises from the value $r = 0.21 \pm 0.03$, corresponding to the free 21-mer, to the value $r \approx 0.3$, corresponding to the anisotropy of the bound oligomer, weighted by the degree of nucleic acid saturation at the applied helicase concentration. As discussed above, the presence of only three relaxation processes in the total emission kinetic traces could indicate that a three-step relaxation process is observed. The broken line in Fig. 7a is a computer simulation of an anisotropy curve using the sequential three-step mechanism and the known anisotropy of the free

nucleic acid. It is evident that the plot does not represent the observed experimental curve. In order to adequately represent the anisotropy data, one would have to assume a much higher steady-state anisotropy of the free 21-mer than experimentally determined.[58] Rather, what is observed is the presence of another fast step, which is not detectable in the total emission experiments, due to very low amplitude, with an intermediate characterized by a high steady-state anisotropy. A nonlinear least-squares fit, using the four-step sequential mechanism [Eq. (8)], provides an excellent description of the observed anisotropy kinetic trace, without introducing any physically unacceptable values of the steady-state anisotropy of any intermediates. Thus, the anisotropy data provide a strong indication that the kinetic mechanism of the ssDNA binding to the total DNA-binding site is at least a four-step mechanism, as defined in Eq. (1) (see Discussion).

The stopped-flow kinetic traces of the fluorescence anisotropy of 21-mer, 5′-Fl-dT(pT)$_{19}$, after mixing the nucleic acid with the RepA hexamer at two different enzyme concentrations in buffer T5 (pH 7.6, 20 °C), are shown in Fig. 7b. The final concentration of the DNA is 5 × 10^{-9} M. The selected final concentrations of the enzyme are 7 × 10^{-7} and 1 × 10^{-6} M, respectively. The analysis of the experimental kinetic traces is greatly facilitated by the fact that F_0, F_1, F_2, F_3, and F_4 and the rate constants for the reaction are known from the total emission studies (see above). We also know the anisotropy of the free 21-mer, r_{D0} = 0.21 ± 0.03. Thus, there are four parameters that must be determined, r_{D1}, r_{D2}, r_{D3}, and r_{D4} [Eq. (7)]. The continuous lines in Fig. 7b are nonlinear least-squares fits of the experimental fluorescence anisotropy curves, using Eq. (8), with anisotropies of the intermediates (H-ssDNA)$_1$, (H-ssDNA)$_2$, (H-ssDNA)$_3$, and (H-ssDNA)$_4$ as fitting parameters. Within experimental accuracy, the values of r_{D1}, r_{D2}, r_{D3}, and r_{D4}, obtained at different protein concentrations, are close, which is an expected result, as at any protein concentration, the same intermediates, characterized by the same steady-state fluorescence anisotropies, are observed. The obtained values of r_{D1}, r_{D2}, r_{D3}, and r_{D4}, averaged over applied protein concentrations, are as follows: r_{D1} = 0.40 ± 0.02, r_{D2} = 0.28 ± 0.02, r_{D3} = 0.28 ± 0.02, and r_{D4} = 0.35 ± 0.02. At 10 °C, the values of the corresponding parameters are as follows: r_{D1} = 0.42 ± 0.02, r_{D2} = 0.33 ± 0.02, r_{D3} = 0.32 ± 0.02, and r_{D4} = 0.38 ± 0.02 (data not shown). These results indicate that the 5′ end of the nucleic acid becomes strongly immobilized in the first intermediate, (H-ssDNA)$_1$. In two subsequent intermediates, (H-ssDNA)$_2$ and (H-ssDNA)$_3$, the mobility of the 5′ end of the bound DNA decreases, while the 5′ end once again becomes strongly immobilized in the final intermediate, (H-ssDNA)$_4$ (see Discussion).

Analogous stopped-flow fluorescence anisotropy experiments have been performed with the ssDNA 21-mer labeled at the 3′ end with fluorescein. The kinetic trace of the fluorescence anisotropy of the 21-mer, dT(pT)$_{19}$-Fl-3′, after mixing the nucleic acid with the RepA hexamer, is shown in Fig. 8a. The final concentrations of the DNA and the enzyme are 5 × 10^{-9} and 1 × 10^{-6} M, respectively. The trace was recorded in the time range from 1 to 2000 s (see above). The broken line in Fig. 8a is a computer simulation of anisotropy curve using the three-step mechanism and the known anisotropy of the free nucleic acid, 0.21 ± 0.03. It is evident that the plot does not represent the observed experimental curve. As we discussed above, in order to adequately represent the anisotropy data, we would have to assume that the steady-state fluorescence anisotropy of the free 21-mer is much higher than experimentally observed. In other words, anisotropy data indicate the presence of another fast step with an intermediate characterized by high fluorescence anisotropy, not detectable in the total emission studies (see above). The continuous line in Fig. 8a is a nonlinear least-squares fit, using the four-step sequential mechanism [Eq. (8)], which provides an adequate description of the observed anisotropy kinetic trace.

The stopped-flow kinetic traces of the fluorescence anisotropy of $dT(pT)_{19}$-Fl-3′, after mixing the oligomer with the RepA hexamer, at three different enzyme concentrations, are shown in Fig. 8b. The selected final concentrations of the enzyme are 5×10^{-7}, 7×10^{-7}, and 1×10^{-6} M. To extract steady-state anisotropies of the reaction intermediates, we analogously analyzed the experimental kinetic curves, as described above for 5′-Fl-$dT(pT)_{19}$. In the case of $dT(pT)_{19}$-Fl-3′, binding of the RepA hexamer is accompanied by a small ~3–5% change of the nucleic acid fluorescence.[12] Therefore, in the analysis of the experimental kinetic traces in Fig. 8b, one can take that $F_0 = F_1 = F_2 = F_3 = F_4 = 1$. Moreover, the rate constants are the same as those obtained for the oligomer labeled at the 5′ end, 5′-Fl-$dT(pT)_{19}$, in the total emission kinetic studies (Table 1). We also know the anisotropy of the free 21-mer, $r_{D0} = 0.21 \pm 0.03$. Nevertheless, there are still four parameters that must be determined, r_{D1}, r_{D2}, r_{D3}, and r_{D4}, that is, the specific steady-state anisotropies of the intermediates $(H\text{-}ssDNA)_1$, $(H\text{-}ssDNA)_2$, $(H\text{-}ssDNA)_3$, and $(H\text{-}ssDNA)_4$. The continuous lines in Fig. 8b are nonlinear least-squares fits of the kinetic anisotropy curves, using Eq. (8). The obtained values of r_{D1}, r_{D2}, r_{D3}, and r_{D4}, averaged over applied protein concentrations, are $r_{D1} = 0.40 \pm 0.02$, $r_{D2} = 0.35 \pm 0.02$, $r_{D3} = 0.36 \pm 0.02$, and $r_{D4} = 0.37 \pm 0.02$. Thus, the behavior of the 3′ end of the nucleic acid in the association reaction with the RepA hexamer is different from that observed for the 5′ end. The 3′ end of $dT(pT)_{19}$-Fl-3′ becomes strongly immobilized in the first intermediate, $(H\text{-}ssDNA)_1$, as observed for 5′-Fl-$dT(pT)_{19}$. However, in the subsequent two intermediates, $(H\text{-}ssDNA)_2$ and $(H\text{-}ssDNA)_3$, the mobility of the 3′ end is still strongly restricted, and it remains in the strongly immobilized state in the final intermediate, $(H\text{-}ssDNA)_4$ (see Discussion).

Discussion

Energetics and dynamics of interactions of the replicative hexameric helicase with the ssDNA play a fundamental role in enzyme activities.[1-7] This includes the specific recognition of the ssDNA conformation of the replication origin, oriC, as well as the mechanism of the free-energy transduction by the enzyme. The complexity of the system is reflected in the fact that, in the equilibrium complex, the ssDNA is bound to the total DNA-binding site, located inside the cross channel of the ringlike structure of the hexamer (Fig. 1). Thus, the stability of the hexameric structure and the dynamics of the conformational flexibility are inherently involved in the protein association with the nucleic acid. Moreover, although the total site size of the hexamer–ssDNA complex of the RepA helicase or the E. coli DnaB is ~20 nucleotides, the corresponding total DNA-binding site of both enzymes is heterogeneous and divided into strong and weak DNA-binding subsites, which encompass a similar number of nucleotides, but differ by orders of magnitude in the affinities for the nucleic acid.[12,26]

Sequential, multiple-step kinetic mechanism of the ssDNA binding to the total DNA-binding site and to the strong DNA-binding subsite of the RepA helicase

In the presence of the ATP nonhydrolyzable analog AMP-PNP, binding of the ssDNA oligomers that encompass the total DNA-binding site and the ssDNA oligomers that exclusively bind to the strong DNA-binding subsite occurs through the same four-step sequential mechanism; that is, three isomerization processes follow the bimolecular association [Eq. (1)]. There are two important aspects of these data. First,the observed independence of the mechanism upon the length of the ssDNA indicates that the observed intermediates of the reaction are generated by the response of the protein to the nucleic acid binding; that is, they are the intrinsic property of the enzyme. Second, the RepA hexamer-ssDNA complex undergoes multiple conformational transitions, indicating that the complex exists in multiple conformational states (see below). The observed mechanism is more complex than that observed for the E. coli DnaB hexamer, which associates with the ssDNA

through a three-step sequential process.[29] The increased complexity of the dynamics of the association process most probably reflects the significantly more stable hexameric structure of the RepA helicase than the analogous hexameric structure of the DnaB protein (see below).[8-14,21,28]

Extreme stability of the RepA hexamer precludes any disintegration of the hexamer into monomers or into lower oligomeric entities.[8-14,21,28] On the other hand, the sequential nature of the kinetic mechanism indicates that the enzyme predominantly exists in a single conformational state prior to the nucleic acid binding.[29,30,35-40] This is further confirmed by the finding that the number of relaxation processes remains the same under pseudo-first-order conditions with respect to the nucleic acid concentration (data not shown).[59] As we previously discussed, if the protein were in different conformations prior to the DNA association, then, under pseudo-first-order conditions with respect to the nucleic acid, the number of relaxation processes would be lower than that observed in the large excess of the protein, a feature that is easy to detect in kinetic experiments.[59] The sequential character of the mechanism may seem surprising, as our hydrodynamic studies, using analytical ultracentrifugation and dynamic light-scattering methods, showed that the RepA hexamer exists in multiple conformational states, generated by a specific and different number of bound nucleotide cofactors, prior to the nucleic acid binding.[21] However, the binding of AMP-PNP to the six, initially independent, nucleotide-binding sites of the RepA hexamer is characterized by strong negative cooperativity.[13,14] At the selected concentration of the AMP-PNP, 0.5 mM, only three nucleotide-binding sites are fully saturated with the cofactor, without engaging in cooperative interactions. In this binding state, the enzyme is predominantly in a single conformation, in which it has an increased affinity for the ssDNA.[21] Therefore, the kinetic results entirely corroborate the previous hydrodynamic data.

Association of the RepA hexamer with the ssDNA proceeds through steps characterized by dramatically different dynamics

Intermediates in the RepA hexamer association with the ssDNA dramatically differ in the dynamics of their formation, both for the association with the total DNA-binding site and the strong DNA-binding subsite (Tables 1 and 2). The first bimolecular step, RepA+ssDNA↔ $(H\text{-}ssDNA)_1$ [Eq. (1)], is beyond detection in the stopped-flow experiments. That would require that the reciprocal relaxation time characterizing this step is ≥ 1000 s, at the selected protein concentrations. Even if the association process was completely diffusion-controlled, the corresponding reciprocal relaxation time mainly reflects the backward rate constant, k_{-1}.[29,30,35-40] The smaller than diffusion-controlled forward rate constant, k_1, would make the reciprocal relaxation time even closer to k_{-1}. Thus, the value of k_{-1} is at least 1000 s^{-1} for the binding to the total binding site and to the strong subsite. Such a fast first step indicates that it involves the initial nucleic acid association with the outside surface of the hexamer, presumably on a single subunit and very fast, local structural rearrangements of the formed complex; that is, it does not involve large global conformational changes of the entire hexamer, analogously to the fast association reactions of the monomeric proteins with the nucleic acid (see below).[60]

The second transition, $(H\text{-}ssDNA)_1 \leftrightarrow (H\text{-}ssDNA)_2$, is ~3 orders of magnitude slower than the first step for both the total DNA-binding site and the strong DNA-binding subsite. The dramatic drop in the rate of the reaction step indicates a dramatic change in the nature of the formed intermediate and strongly suggests that the dynamics of the $(H\text{-}ssDNA)_2$ formation reflects the opening of the large hexameric structure of the RepA helicase. This conclusion is further supported by very different changes of enthalpy and entropy for the formation of $(H\text{-}ssDNA)_2$, as compared to enthalpy of formation of $(H\text{-}ssDNA)_1$ (see below). In the case of the ssDNA oligomers that engage the total DNA-binding site, the values of the rate constant, $k_2 \approx 3\ s^{-1}$, indicate that the opening occurs within ~300 ms. Notice that this

transition is directly seen in the case of the extremely stable RepA hexamer but was not detectable in the association with the nucleic acid of the analogous but less stable *E. coli* DnaB hexamer.[29,30] Nevertheless, we could estimate the corresponding rate constant for the DnaB hexamer[29] and obtained ~3.4 s^{-1}. Thus, the dynamics of the opening of the hexameric structure, when the enzyme associates with the ssDNA that encompasses the total DNA-binding site, seems to be very similar among the replicative hexameric helicases.

The values of the rate constants k_2 and k_{-2} are higher by approximately a factor of 6 for the oligomers that exclusively bind to the strong DNA-binding site (Tables 1 and 2). Such a difference, which depends on the length of the bound DNA, points to a different engagement of the shorter oligomers in interactions with the protein both in $(H\text{-}ssDNA)_1$ and $(H\text{-}ssDNA)_2$ intermediates, which overlaps with the proposed process of the opening of the hexameric structure, $(H\text{-}ssDNA)_1 \leftrightarrow (H\text{-}ssDNA)_2$ (see below). It also indicates that the intrinsic rate of the hexamer opening may be even faster than that observed for the longer oligomers and occurs within ~50 ms. The rates of the final two transitions, $(H\text{-}ssDNA)_2 \leftrightarrow (H\text{-}ssDNA)_3$ and $(H\text{-}ssDNA)_3 \leftrightarrow (H\text{-}ssDNA)_4$, are ~2–3 orders of magnitude slower than the transition $(H\text{-}ssDNA)_1 \leftrightarrow (H\text{-}ssDNA)_2$. Once again, the slow pace of the transitions indicates that they involve large conformational changes of the entire hexamer. On the other hand, the different dynamics of both final steps, observed for the short versus long oligomers, points to a different engagement of the oligomers that encompass the total binding site and the strong subsite, in interactions with the protein in intermediates $(H\text{-}ssDNA)_3$ and $(H\text{-}ssDNA)_4$. The shorter oligomers can enter the $(H\text{-}ssDNA)_3$ intermediate as easily as the longer nucleic acid. However, as we pointed out above, it is more difficult for the shorter oligomers to return to the $(H\text{-}ssDNA)_2$ intermediate than for the longer oligomers. On the other hand, the higher rate constant k_{-4} for the shorter oligomers indicates that they can leave the $(H\text{-}ssDNA)_4$ intermediate, back to the $(H\text{-}ssDNA)_3$, easier than the oligomers that can engage the total DNA-binding site (see below).

In the ssDNA association with the RepA helicase, the binding steps are characterized by different apparent enthalpy and entropy changes than the accompanying conformational changes of the hexamer

Temperature effect on the binding of the RepA hexamer to the ssDNA provides an additional, strong indication of the different nature of the formed intermediates. The first reaction step is characterized by the apparent negative enthalpy and entropy changes for both oligomers that engage the total DNA-binding site and that exclusively bind to the strong DNA-binding subsite (Table 3). In both cases, the first step, $RepA+ssDNA \leftrightarrow (H\text{-}ssDNA)_1$, must include the fast association of the nucleic acid and the fast local rearrangement of the binding site (see above). Thus, the data show that the intrinsic DNA-binding process of the RepA hexamer, independent of the length of the nucleic acid, apparently is an enthalpy-driven process. The accompanying enthalpy changes are significantly larger than expected for a simple diffusion-controlled reaction, indicating that the observed first step indeed includes structural changes of the formed complex.[40,61] The following transition, $(H\text{-}ssDNA)_1 \leftrightarrow (H\text{-}ssDNA)_2$,is very different from the bimolecular step and is characterized by apparent positive enthalpy and entropy changes, for both the oligomers that engage the total DNA-binding site and the oligomers that exclusively bind to the strong DNA-binding subsite (Table 3).

As discussed above, dramatically slower dynamics of the second step for both sets of ssDNA oligomers, as compared to the bimolecular step, indicates that a global conformational change of the RepA hexamer, that is, the opening of the hexameric structure, is dominating this transition (see above). The equally dramatic changes in the signs of the thermodynamic functions strongly support the conclusion that a process of a different nature dominates the step $(H\text{-}ssDNA)_1 \leftrightarrow (H\text{-}ssDNA)_2$. Thus, the data indicate that the opening of

the hexameric structure of the RepA helicase is an entropy-driven process strongly opposed by the enthalpy changes. Such thermodynamic characteristics of the hexameric structure energetics can be understood if one takes into account the extreme stability of the RepA hexamer, which requires perfectly matching protein–protein interfaces, with multiple and energetically favorable interactions. Breaking such intersubunit engagements must be energetically unfavorable. Moreover, a large positive entropy change also suggests that the reorientation of subunits in the transition $(\text{H-ssDNA})_1 \leftrightarrow (\text{H-ssDNA})_2$ is accompanied by large changes in the hydration of the hexamer. This conclusion corroborates our findings that global conformation changes of the RepA hexamer are accompanied by large changes of the degree of hydration, which contribute to changes in the partial specific volume of the enzyme.[21]

The next step, $(\text{H-ssDNA})_2 \leftrightarrow (\text{H-ssDNA})_3$, is different for the ssDNA oligomers that engage the total DNA-binding site, as compared to the oligomers that exclusively bind to the strong DNA-binding subsite. For the longer oligomers, the transition is accompanied by apparent positive enthalpy and entropy changes, ΔH_3 and ΔS_3, while for the shorter oligomers, the process is characterized by apparent negative changes of the corresponding thermodynamic functions (Table 3). A plausible explanation of this difference is that, in the case of the ssDNA oligomers that engage the total binding site, the entry of the nucleic acid into the cross channel requires further enlargement of the opening of the hexameric structure, which is energetically unfavorable, without involving the changes in the state of the bound DNA. This conjecture is supported by the fluorescence anisotropy data on the entry of the 21-mer into the hexamer (see below). In the case of the shorter oligomers, the additional global structural changes are not necessary and the short DNA oligomer enters the cross channel, engaging one of the strong ssDNA-binding subsites.[12] The DNA-binding process is intrinsically characterized by negative enthalpy and entropy changes, analogous to the formation of the initial intermediate, $(\text{H-ssDNA})_1$ (see above), resulting in the observed apparent negative enthalpy and entropy changes for the process (see above). The final step, $(\text{H-ssDNA})_3 \leftrightarrow (\text{H-ssDNA})_4$, is similar for both sets of ssDNA oligomers and is characterized by apparent negative changes of ΔH_4 and ΔS_4 (Table 3). This step must include the association of the longer oligomers with the total DNA-binding site, which is characterized by negative enthalpy and entropy changes, analogous to the formation of $(\text{H-ssDNA})_1$ and, at least, partial closing of the hexameric structure, which is also driven by negative enthalpy change, as opposed to its opening (see above). In the case of the shorter oligomers that are already engaged in interactions with the strong DNA-binding subsite, the step predominantly includes the enthalpy-driven partial closing of the hexameric structure, resulting in the observed apparent negative enthalpy and entropy changes (Table 3).

The RepA hexamer remains in the partially open state in the equilibrium tertiary complex RepA hexamer–ssDNA–AMP-PNP

The first indication that the equilibrium complex of the RepA hexamer with the ssDNA is a mixture of different conformational states comes from the analysis of the fractional distributions of different intermediates of the reaction. The plots in Fig. 5, generated using the determined kinetic parameters, indicate that, at equilibrium, the population of the tertiary complex RepA hexamer–ssDNA–AMP-PNP is dominated by two intermediates, $(\text{H-ssDNA})_3$ and $(\text{H-ssDNA})_4$. This is true for the 21-mer, which encompasses the total DNA-binding site, and for the 11-mer, which exclusively engages the strong DNA-binding subsite. Recall that the kinetic and thermodynamic results discussed above strongly suggest that the largest opening of the hexameric structure occurs in the intermediate $(\text{H-ssDNA})_3$, while $(\text{H-ssDNA})_4$ is either closed or in a partially open state, resembling the global structure of the RepA hexamer in the binary complex RepA–AMP-PNP. Therefore, the average global conformation of the equilibrium tertiary complex should be different from the global

conformation of the RepA hexamer in the binary complex. Analytical sedimentation velocity data very strongly support this conclusion.

The apparent average sedimentation coefficients of both tertiary complexes with the ssDNA 21-mer and 11-mer are dramatically larger than those determined for the RepA hexamer in the binary complex, showing that the average global conformation of the RepA hexamer in the equilibrium tertiary complex is indeed very different from its conformation in the binary complex. In the binary complex RepA hexamer–AMP-PNP and in the presence of 0.5 mM AMP-PNP, the apparent average sedimentation coefficient ($s_{20,w}$) of the RepA hexamer is 8.5±0.1 S, which indicates that the hexamer has an axial ratio (p) of ~1.9, when modeled as an oblate ellipsoid of revolution.[21] The obtained values of the apparent average sedimentation coefficients for tertiary complexes with the 21- and 11-mer are $s_{20,w}$ = 10.0±0.1 S and $s_{20,w}$ = 9.8±0.1 S, respectively, indicating that the hexamer becomes much more spherical.[21] This would be expected for the open intermediate, (H-ssDNA)$_3$. In other words, a large population of the equilibrium tertiary complex of the RepA hexamer with the ssDNA and the ATP nonhydrolyzable analog AMP-PNP exists in a conformational state with an open hexameric structure. At present, we cannot exclusively address the global conformation of the intermediate (H-ssDNA)$_4$. However, the values of the apparent average sedimentation coefficients of both examined tertiary complexes strongly suggest that the structure of (H-ssDNA)$_4$ is also more spherical than that in the binary complex and possibly is in the partially open state.

The RepA hexamer possesses an outer DNA-binding site located outside the cross channel of the ringlike hexameric structure

The plots of the fractional distributions of the reaction intermediates (Fig. 5) indicate that the fast-formed intermediate (H-ssDNA)$_1$ sustains over a large time span of the association process for the ssDNA oligomers that engage the total DNA-binding sites and the oligomers that bind to the strong DNA-binding subsite. Moreover, the values of ΔH_1 and ΔS_1 indicate that formation of (H-ssDNA)$_1$ is not a simple diffusion-controlled process but involves energetically favorable conformational rearrangement of the complex. Furthermore, the fluorescence anisotropy data show that the nucleic acid is strongly immobilized in (H-ssDNA)$_1$ (see below). Thus, the data strongly indicate that the RepA hexamer possesses a DNA-binding site located outside the cross channel of the hexamer, which forms the initial complex with the nucleic acid. The outside location of the site results in similar environment around the fluorescent marker, resulting in an unchanged value of the fluorescence emission (Tables 1 and 2). As pointed out above, this is different from the large fluorescence changes of the etheno derivative of the ssDNA 20-mer, dεA(pεA)$_{19}$, observed for the first intermediate in the association of the analogous E. coli DnaB hexamer with the ssDNA.[29] First, the identified first step of the E. coli DnaB–ssDNA interactions includes the step that we were able to identify for the RepA hexamer as the transition (H-ssDNA)$_1$↔(H-ssDNA)$_2$. Second, the etheno derivative fluorescence monitors the structure of the entire bound ssDNA oligomer, while the fluorescein marker reports local environment of the part of the bound nucleic acid at its 5′ end.

Because the RepA hexamer is composed of six identical subunits, each subunit must possess an outer DNA-binding site. At first, this may seem odd with the fact that thermodynamic equilibrium studies have clearly shown that only a single molecule of the ssDNA 21-mer binds to the RepA hexamer.[12] However, all transitions of the formed complex, subsequent to the formation of the intermediate (H-ssDNA)$_1$, are characterized by favorable changes of the free energy of binding (Tables 1 and 2). As a result, the final equilibrium is strongly shifted from the intermediate (H-ssDNA)$_1$ toward the following intermediates. The plots in Fig. 5 show that the intermediate (H-ssDNA)$_1$ constitutes only a minute fraction, ~1–3%, of the

equilibrium complex. Within experimental accuracy, such a small presence of the initial complex would not be detectable in standard equilibrium experiments.

A puzzling aspect of the association of the ssDNA oligomers that engage the total DNA-binding site of the RepA hexamer is the lack of the statistical effect, even in the formation of the initial complex $(H\text{-}ssDNA)_1$ (Table 1). As pointed out above, such a statistical effect is expected in the large protein binding to the homogeneous nucleic acid lattice.[41-44] The statistical effect is clearly seen in the binding of the oligomers that engage the strong DNA-binding subsite (Table 2). Moreover, as expected, the statistical effect is entirely expressed in the formation of the first intermediate, $(H\text{-}ssDNA)_1$. However, as discussed above, the formation of the intermediate $(H\text{-}ssDNA)_1$ includes an additional rearrangement of the formed complex, which may depend upon the length of the associated nucleic acid. Recall that while the binding to the strong DNA-binding subsite is base-independent, the binding of the oligomers that engage the total DNA-binding site is dependent upon the base composition of the nucleic acid; that is, it shows a significant preference for pyrimidine oligomers.[12] Because the major part of the free energy of binding is generated in the bimolecular step (see above), the obtained results indicate that the outer DNA-binding site of the RepA hexamer possesses an ability to discriminate between oligomers of different base compositions. In other words, the conformational rearrangement of the initial complex with the longer ssDNA oligomers is different from the shorter oligomer and may mask the expected statistical effect. Moreover, the notion that the base/sequence specificity for long oligomers is already in the outside binding site is further supported by the similarity in the energetics of the next steps of the reaction for the longer and shorter ssDNA oligomers (Tables 1 and 2). If the base specificity were tested in the steps following the formation of $(H\text{-}ssDNA)_1$, a significant difference in the energetics of some of these steps between the long and short oligomers would be manifested and this has not been experimentally observed.

Steady-state fluorescence anisotropies of the reaction intermediates indicate a different engagement of the 5′ and 3′ ends of the ssDNA oligomers during the course of the association reaction: Model for the RepA hexamer association with the ssDNA

The analysis of the stopped-flow kinetic data using fluorescence anisotropy provided invaluable information about the mechanism of the examined reaction.[38,57] This is due to the fact that the anisotropy records formation of intermediates, which may not be accompanied by detectable amplitudes in the fluorescence intensity measurements. Yet, they may differ in their mobilities.[57] In the case of the RepA hexamer–ssDNA association, it allowed us to formulate the correct kinetic mechanism of the observed association process. The difference in the steady-state anisotropies of the reaction intermediates, in the binding of the RepA hexamer to the ssDNA oligomers, labeled at the 5′ or 3′ end of the nucleic acids and encompassing the total DNA-binding site of the enzyme, is striking. The anisotropy of the first intermediate, $(H\text{-}ssDNA)_1$, is $r_{D1} = 0.40\pm0.02$ for both 5′-Fl-$dT(pT)_{19}$ and $dT(pT)_{19}$-Fl-3′. Because the theoretically largest possible anisotropy value is 0.4, these data indicate that in the first formed complex, the entire 21-mer is strongly immobilized, reinforcing the notion that $(H\text{-}ssDNA)_1$ is not a simple collision complex, in spite of the fact that there is no fluorescence intensity change accompanying the formation of the first intermediate (Table 1). However, in the next two intermediates, $(H\text{-}ssDNA)_2$ and $(H\text{-}ssDNA)_3$, the steady-state anisotropies of 5′-Fl-$dT(pT)_{19}$ are $r_{D2} = 0.28 \pm 0.02$ and $r_{D3} = 0.28\pm0.02$, while the analogous values of the steady-state anisotropies are $r_{D2}=0.35\pm0.02$ and $r_{D3} = 0.36\pm0.02$ for $dT(pT)_{19}$-Fl-3′. Therefore, in both intermediates $(H\text{-}ssDNA)_2$ and $(H\text{-}ssDNA)_3$, the 5′ end of the nucleic acid regains significant mobility, while the 3′ end remains strongly immobilized. Moreover, the fluorescence intensity of the marker at the 5′ end is quenched, indicating an environment change around the 5′ end, while the analogous

fluorescence intensity of the marker at the 3′ end is slightly affected. In the final intermediate, $(H\text{-}ssDNA)_4$, the anisotropies are r_{D4}=0.35±0.02 and r_{D4} = 0.37±0.02, for the 5′ and 3′ end, respectively, indicating that the entire nucleic acid is once again strongly immobilized.

The fluorescence anisotropy and hydrodynamic, kinetic, spectroscopic, and energetic analyses discussed above provide a plausible model for the association of the RepA hexamer with the ssDNA that encompasses the total DNA-binding site and the entry of the nucleic acid into the cross channel of the helicase. The model is depicted in Fig. 9. Association of the DNA with the outer DNA-binding site, on one of the hexamer subunits, leads to the formation of the initial complex, $(H\text{-}ssDNA)_1$, in which the entire nucleic acid, that is, both 5′ and 3′ ends, is strongly immobilized. The hexameric structure of the enzyme remains closed in this complex and the global structure of the enzyme is characterized by an axial ratio of p~1.9.[21] In the next intermediate, $(H\text{-}ssDNA)_2$, the hexameric structure becomes locally open and part of the bound nucleic acid, from its 5′ end, enters the cross channel. The environment around the 5′ end changes as indicated by quenching of the fluorescein marker emission. Nevertheless, the DNA cannot yet engage the total DNA-binding site inside the cross channel. As a result, the 5′ end of the nucleic acid regains significant mobility. In the same complex, the DNA fragment in the vicinity of the 3′ end stays bound to the outer DNA-binding site and is strongly immobilized. The environment around the 3′ end remains unchanged, resulting in very little change in the intensity of the fluorescein marker emission. In the following intermediate, $(H\text{-}ssDNA)_3$, the opening of the hexameric structure widens without significantly affecting the state of the bound DNA, with the mobility and the environment of the 5′ and 3′ ends remaining very similar to the their mobility in $(H\text{-}ssDNA)_2$; that is, the 5′ end has significant mobility, while the 3′ end remains immobilized. The global structure of the open hexamer becomes much more spherical. In the final intermediate, $(H\text{-}ssDNA)_4$, the nucleic acid fully enters the cross channel and forms all contacts with the total DNA-binding site inside the cross channel. The hexameric structure closes over the bound DNA, although possibly, only partially.

Materials and Methods

Reagents and buffers

All solutions were made with distilled and deionized >18 MΩ (Milli-Q Plus) water. All chemicals were of reagent grade. Buffer T5 is 50 mM Tris adjusted to pH 7.6 with HCl at a given temperature, 1 mM $MgCl_2$, 10mM NaCl, and 10% glycerol. The temperature in the buffer is indicated in the text.

RepA helicase of plasmid RSF1010

Isolation and purification of the protein were performed, with slight modifications, as previously described.[12-14] The protein was >99% pure as judged by SDS acrylamide gel electrophoresis with Coomassie Brilliant Blue staining. The concentration of the protein was spectrophotometrically determined using the extinction coefficient $\varepsilon_{280}=1.656 \times 10^5\ cm^{-1}\ M^{-1}$, obtained with approach based on Edelhoch's method.[62,63]

Nucleic acids

All nucleic acids were purchased from Midland Certified Reagents (Midland, TX). The ssDNA oligomers with fluorescein at the 5′ end were synthesized using fluorescein phosphoramidate. Labeling of the oligomers at the 3′ end with fluorescein was performed by synthesizing the oligomer with a nucleotide residue with the amino group on a six-carbon linker and, subsequently, modifying the amino group with fluorescein 5′-isothiocyanate (Midland, TX). The degree of labeling was determined by absorbance at 494 nm for

fluorescein (pH 9) using the extinction coefficient, ε_{494}=7.6 × 10^4 M^{-1} cm^{-1} [12,26,28,52,58] Concentrations of all ssDNA oligomers have been spectrophotometrically determined, as previously described by us.[12,26,28,52,58]

Analytical ultracentrifugation measurements

Sedimentation velocity experiments were performed with an Optima XL-A analytical ultracentrifuge (Beckman Inc., Palo Alto, CA) using double-sector charcoal-filled 12-mm centerpieces, as we previously described.[10,12,15,27,33,34,52-54] Sedimentation velocity scans were collected at the absorption band of the fluorescein marker at 495 nm. Time-derivative analysis of the scans was performed with the software supplied by the manufacturer. The values of the apparent average sedimentation coefficients were corrected to $s_{20,w}$ for solvent viscosity and temperature to standard conditions.[48,49]

Stopped-flow kinetics

All fluorescence stopped-flow kinetic experiments were performed using an SX.MV18 stopped-flow instrument (Applied Photophysics Ltd. Leatherhead, UK). The reactions were monitored using the total fluorescence of the fluorescein-labeled ssDNA oligomers with λ_{ex}=475 nm, and the emission was observed through a GG500 cutoff filter (Schott, Pennsylvania), with the excitation monochromator slits at 1 mm (band pass ~4.5 nm). The sample was excited with the vertically polarized light, and the time development of the function

$$F(t) = I_{VV}(t) + 2GI_{VH}(t) \tag{9}$$

was monitored, where I_{VV} is the fluorescence intensity and the first and second subscripts refer to vertical (V) polarization of the excitation and vertical (V) or horizontal (H) polarization of the emitted light. The factor $G = I_{HV}/I_{HH}$ corrects for the different sensitivity of the emission monochromator for vertically and horizontally polarized light.[38] The experiments were performed in the oversampling mode, in which the instrument collects and averages the multiple data points at the fastest instrumental rate for the selected time interval, achieving a higher signal-to-noise ratio. Usually, five to seven traces were collected and averaged for each sample. The kinetic curves were fitted to extract relaxation times and amplitudes using nonlinear least-squares software provided by the manufacturer, with the exponential function defined as

$$F(t) = F(\infty) + \sum_{i=1}^{n} A_i \exp(-\lambda_i t) \tag{10}$$

where $F(t)$ is the fluorescence intensity at time t, $F(\infty)$is the fluorescence intensity at $t=\infty$, A_i is the amplitude corresponding to the ith relaxation process, λ_i is the reciprocal relaxation time characterizing the ith relaxation process, and n is number of relaxation processes. All analyses of the data were performed using Mathematica (Wolfram, Urbana, IL) and KaleidaGraph (Synergy Software, Pennsylvania).

Analysis of stopped-flow kinetic experiments

Quantitative examinations of both the relaxation times and the amplitudes of the observed kinetic processes have been performed using the matrix projection operator approach.[22,23,29,30,33,36,37,39] The mechanism of the ssDNA (D) binding to the RepA hexamer (H) includes the bimolecular step, which is followed by three first-order conformational transitions as

$$H+D_0 \underset{k_{-1}}{\overset{k_1}{\rightleftarrows}} D_1 \underset{k_{-2}}{\overset{k_2}{\rightleftarrows}} D_2 \underset{k_{-3}}{\overset{k_3}{\rightleftarrows}} D_3 \underset{k_{-4}}{\overset{k_4}{\rightleftarrows}} D_4 \tag{11}$$

For simplicity, here we use symbols H and D for the enzyme and the nucleic acid intermediates. The reaction is monitored by the fluorescence change of the nucleic acid. The differential equations describing the time course of Eq. (11), in terms of the different nucleic acid species (D_0, D_1, D_2, D_3, D_4), are, in matrix notation, defined as

$$\begin{pmatrix} \frac{dD_0}{dt} \\ \frac{dD_1}{dt} \\ \frac{dD_2}{dt} \\ \frac{dD_3}{dt} \\ \frac{dD_4}{dt} \end{pmatrix} = \begin{pmatrix} -k_1[\mathrm{H}] & k_{-1} & 0 & 0 & 0 \\ k_1[\mathrm{H}] & -(k_{-1}+k_2) & k_{-2} & 0 & 0 \\ 0 & k_2 & -(k_{-2}+k_3) & k_3 & 0 \\ 0 & 0 & k_3 & -(k_3+k_4) & -k_{-4} \\ 0 & 0 & 0 & k_4 & k_{-4} \end{pmatrix} \begin{pmatrix} D_0 \\ D_1 \\ D_2 \\ D_3 \\ D_4 \end{pmatrix} \tag{12}$$

and

$$\dot{\mathbf{D}} = \mathbf{M}\mathbf{D} \tag{13}$$

where $\dot{\mathbf{D}}$ is a vector of time derivatives, **M** is the coefficient matrix, and **D** is the vector of concentrations of different nucleic acid species in solution. The solution of Eq. (12) is then

$$\mathbf{D} = \exp(\mathbf{M}t)\,\mathbf{D}_0 \tag{14}$$

where

$$\exp(\mathbf{M}t) = \mathbf{V} \begin{pmatrix} \exp(\lambda_0 t) & 0 & 0 & 0 & 0 \\ 0 & \exp(\lambda_1 t) & 0 & 0 & 0 \\ 0 & 0 & \exp(\lambda_2 t) & 0 & 0 \\ 0 & 0 & 0 & \exp(\lambda_3 t) & 0 \\ 0 & 0 & 0 & 0 & \exp(\lambda_4 t) \end{pmatrix} \mathbf{V}^{-}1 \tag{15}$$

Quantities λ_0, λ_1, λ_2, λ_3, and λ_4 are eigenvalues of matrix **M**, **V** is a matrix whose columns are the eigenvectors of matrix **M**, and $\mathbf{D}_0$ is the vector of the initial concentrations. In the considered case of the sequential reaction, defined in Eq. (2), $\mathbf{D}_0$ is a column vector, (D_T, 0,0, 0,0), where, D_T is the total concentration of the nucleic acid. The matrix, exp(**M***t*) can be expanded using its eigenvalues, exp($\lambda_i t$), and corresponding projection operators, $\mathbf{Q_i}$, as[22,23,29,30,33,36,37,39]

$$\exp(\mathbf{M}t) = \sum_{i=0}^{4} \mathbf{Q_i} \exp(\lambda_i t) \tag{16}$$

The projection operators, $\mathbf{Q_i}$, are analytically defined using the original coefficient matrix **M** and its eigenvalues, λ_i, by Sylvester's theorem, as[64,65]

$$\mathbf{Q_i}=\frac{\prod_{j\neq i}^{n}\left(\mathbf{M}-\lambda_j\mathbf{I}\right)}{\prod_{j\neq i}^{n}\left(\lambda_i-\lambda_j\right)} \tag{17}$$

where n is the number of eigenvalues and **I** is the identity matrix of the same size as **M**. In the considered case, there are five eigenvalues, λ_0, λ_1, λ_2, λ_3,and λ_4. One eigenvalue, $\lambda_0 = 0$, results from the mass conservation in the reaction system at equilibrium. The solution for the system of Eq. (3) is then

$$\mathbf{D}=\mathbf{Q}_0\mathbf{D}_0+\mathbf{Q}_1\mathbf{D}_0\exp(\lambda_1 t)+\mathbf{Q}_2\mathbf{D}_0\exp(\lambda_2 t)+\mathbf{Q}_3\mathbf{D}_0\exp(\lambda_3 t)+\mathbf{Q}_4\mathbf{D}_0\exp(\lambda_4 t) \tag{18}$$

The products $\mathbf{Q_iD_0}$ are column vectors, $\mathbf{P_i}$, which are the projections of $\mathbf{D_0}$ on each eigenvector of matrix **M** that is,

$$\begin{pmatrix} D_0\\ D_1\\ D_2\\ D_3\\ D_4 \end{pmatrix}=\begin{pmatrix} P_{01}\\ P_{02}\\ P_{03}\\ P_{04}\\ P_{05} \end{pmatrix}+\begin{pmatrix} P_{11}\\ P_{12}\\ P_{13}\\ P_{14}\\ P_{15} \end{pmatrix}\exp(\lambda_1 t)+\begin{pmatrix} P_{21}\\ P_{22}\\ P_{23}\\ P_{24}\\ P_{25} \end{pmatrix}\exp(\lambda_2 t)+\begin{pmatrix} P_{31}\\ P_{32}\\ P_{33}\\ P_{34}\\ P_{35} \end{pmatrix}\exp(\lambda_3 t)+\begin{pmatrix} P_{41}\\ P_{42}\\ P_{43}\\ P_{44}\\ P_{45} \end{pmatrix}\exp(\lambda_4 t) \tag{19}$$

where P_{ij} is the jth element of the projection of the vector of the initial concentrations of $\mathbf{N}_0$ on the eigenvector corresponding to the *i*th eigenvalue of the matrix **M**.

There are five molar fluorescence intensities, F_0, F_1, F_2, F_3, and F_4, characterizing D_0, D_1, D_2, D_3, and D_4 states of the nucleic acid, free and in the complex with the RepA helicase. The fluorescence of the system at any time of the reaction, $F(t)$, is defined as

$$F(t)=F_0D_0+F_1D_1+F_2D_2+F_3D_3+F_4D_4 \tag{20}$$

Introducing Eq. (19) into Eq. (20) and rearranging provides

$$F(t)=\begin{pmatrix} F_0 & F_1 & F_2 & F_3 & F_4 \end{pmatrix}\times\begin{pmatrix} P_{01} & P_{11} & P_{21} & P_{31} & P_{41}\\ P_{02} & P_{12} & P_{22} & P_{32} & P_{42}\\ P_{03} & P_{13} & P_{23} & P_{33} & P_{43}\\ P_{04} & P_{14} & P_{24} & P_{34} & P_{44}\\ P_{05} & P_{15} & P_{25} & P_{35} & P_{45} \end{pmatrix}\begin{pmatrix} 1\\ \exp(\lambda_1 t)\\ \exp(\lambda_2 t)\\ \exp(\lambda_3 t)\\ \exp(\lambda_4 t) \end{pmatrix} \tag{21}$$

The four normal modes of reaction are characterized by the corresponding relaxation times, $\tau_1 = -1/\lambda_1$, $\tau_2 = -1/\lambda_2$, $\tau_3 = -1/\lambda_3$, and $\tau_4 = -1/\lambda_4$, and four amplitudes, A_1, A_2, A_3, and A_4.[22,23,29,30,33,36,37,39] The individual amplitudes contain contributions from the fluorescence intensities characterizing all nucleic acid intermediates of the reaction. The experimental total amplitude, A_T, is defined as

$$A_T=F(0)-F(\infty) \tag{22}$$

where $F(0)$ and $F(\infty)$ are the observed fluorescence intensities, $F(t)$, of the system at $t = 0$ and $t = \infty$, respectively. Introducing $t = 0$ for $F(0)$ and $t = \infty$ for $F(\infty)$ into Eq. (22), subtracting, and rearranging, one obtains the total amplitude, A_T, as

$$A_T = \begin{pmatrix} F_0 & F_1 & F_2 & F_3 & F_4 \end{pmatrix} \begin{pmatrix} P_{11} & P_{21} & P_{31} & P_{41} \\ P_{12} & P_{22} & P_{32} & P_{42} \\ P_{13} & P_{23} & P_{33} & P_{43} \\ P_{14} & P_{24} & P_{34} & P_{44} \\ P_{15} & P_{25} & P_{35} & P_{45} \end{pmatrix} \begin{pmatrix} 1 \\ 1 \\ 1 \\ 1 \end{pmatrix} \quad (23)$$

which is the sum of the individual amplitudes of all normal modes, that is, $A_T = A_1+A_2+A_3+A_4$, where each of the individual amplitudes, A_1, A_2, A_3, and A_4, is a product of the row vector (F_0, F_1, F_2, F_3, F_4), with the corresponding column in Eq. (23).[22,23,29,30,33,36,37,39] The final vector multiplication in Eq. (23) returns the scalar value for the total amplitude.

Acknowledgments

We wish to thank Gloria Drennan Bellard for her help in preparing the manuscript.

Abbreviations used

AMP-PNP	β,γ-imidoadenosine-5′-triphosphate
ssDNA	single-stranded DNA

References

1. Enemark EJ, Joshua-Tor L. On helicases and other motor proteins. Curr. Opin. Struct. Biol. 2008; 18:243–257. [PubMed: 18329872]
2. von Hippel PH, Delagoutte E. Helicase mechanisms and the coupling of helicases within macromolecular machines. Part I: structures and properties of isolated helicases. Q. Rev. Biophys. 2002; 35:431–478. [PubMed: 12621862]
3. von Hippel PH, Delagoutte E. Helicase mechanisms and the coupling of helicases within macromolecular machines. Part II: integration of helicases into cellular processes. Q. Rev. Biophys. 2003; 36:1–69. [PubMed: 12643042]
4. Lohman TM, Bjornson KP. Mechanisms of helicase-catalyzed DNA unwinding. Annu. Rev. Biochem. 1996; 65:169–214. [PubMed: 8811178]
5. Baker TA, Funnell BE, Kornberg A. Helicase action of dnaB protein during replication from the *Escherichia coli* chromosomal origin *in vitro*. J. Biol. Chem. 1987; 262:6877–6885. [PubMed: 3032979]
6. Heller RC, Marians KJ. Non-replicative helicases at the replication fork. DNA Repair. 2007; 6:945–952. [PubMed: 17382604]
7. LeBowitz JH, McMacken R. The *Escherichia coli* dnaB replication protein is a DNA helicase. J. Biol. Chem. 1986; 261:4738–4748. [PubMed: 3007474]
8. Scherzinger E, Ziegelin G, Barcena M, Carazo JM, Lurz R, Lanka E. The RepA protein of plasmid RSF1010 is a replicative DNA helicase. J. Biol. Chem. 1997; 2:30228–30236. [PubMed: 9374507]
9. Niedenzu T, Roleke D, Bains G, Scherzinger E, Saenger W. Crystal structure of the hexameric replicative helicase RepA of plasmid RSF1010. J. Mol. Biol. 2001; 306:479–487. [PubMed: 11178907]
10. De Gaaf J, Crossa JH, Heffron F, Falkow S. Replication of the nonconjugative plasmid RSF1010 in *Escherichia coli* K-12. J. Bacteriol. 1978; 134:1117–1122. [PubMed: 350840]

11. Guerry P, van Embden J, Falkow S. Molecular nature of two nonconjugative plasmids carrying drug resistance genes. J. Bacteriol. 1974; 117:987–997. [PubMed: 4591964]
12. Jezewska MJ, Galletto R, Bujalowski W. Interactions of the RepA helicase hexamer of plasmid RSF1010 with the ssDNA. Quantitative analysis of stoichiometries, intrinsic affinities, cooperativities, and heterogeneity of the total ssDNA-binding site. J. Mol. Biol. 2004; 343:115–136. [PubMed: 15381424]
13. Jezewska MJ, Lucius AL, Bujalowski W. Binding of six nucleotide cofactors to the hexameric helicase RepA protein of plasmid RSF1010. I. Direct evidence of cooperative interactions between the nucleotide-binding sites of a hexameric helicase. Biochemistry. 2005; 44:3865–3876. [PubMed: 15751962]
14. Jezewska MJ, Lucius AL, Bujalowski W. Binding of six nucleotide cofactors to the hexameric helicase RepA protein of plasmid RSF1010. II. Base specificity, nucleotide structure, magnesium, and salt effect on the cooperative binding of the cofactors. Biochemistry. 2005; 44:3877–3890. [PubMed: 15751963]
15. Bujalowski W, Klonowska MM, Jezewska MJ. Oligomeric structure of *Escherichia coli* primary replicative helicase DnaB protein. J. Biol. Chem. 1994; 269:31350–31358. [PubMed: 7989299]
16. Jezewska MJ, Kim U-S, Bujalowski W. Binding of *Escherichia coli* primary replicative helicase DnaB protein to single-stranded DNA. Long-range allosteric conformational changes within the protein hexamer. Biochemistry. 1996; 35:2129–2145. [PubMed: 8652555]
17. Dong F, Gogol EP, von Hippel PH. The phage T4-coded DNA replication helicase (gp41) forms a hexamer upon activation by nucleoside triphosphate. J. Biol. Chem. 1995; 270:7462–7473. [PubMed: 7706292]
18. Gogol EP, Seifried SE, von Hippel PH. Structure and assembly of the *Escherichia coli* transcription termination factor rho and its interactions with RNA. I. Cryoelectron microscopy studies. J. Mol. Biol. 1991; 221:1127–1138. [PubMed: 1719215]
19. Trakselis MA, McGeoch AT, Laskey RA, Bell SD. Organization of the archaeal MCM complex on DNA and implications for the helicase mechanisms. Nat. Struct. Mol. Biol. 2005; 12:756–762. [PubMed: 16116441]
20. Egelman EH, Yu X, Wild R, Hingorani MM, Patel SS. Bacteriophage T7 helicase/primase proteins form rings around single-stranded DNA that suggest a general structure for hexameric helicases. Proc. Natl Acad. Sci. USA. 1995; 92:3869–3873.
21. Marcinowicz A, Jezewska MJ, Bujalowski W. Multiple global conformational states of the hexameric RepA helicase of plasmid RSF1010 with different ssDNA-binding capabilities are induced by different numbers of bound nucleotides. Analytical ultracentrifugation and dynamic light scattering studies. J. Mol. Biol. 2008; 375:386–408. [PubMed: 18022636]
22. Galletto R, Jezewska MJ, Bujalowski W. Unzipping mechanism of the double-stranded DNA unwinding by a hexameric helicase. I. Quantitative analysis of the rate of the dsDNA unwinding, processivity and kinetic step-size of the *Escherichia coli* DnaB helicase using rapid quench-flow method. J. Mol. Biol. 2004; 343:83–99. [PubMed: 15381422]
23. Galletto R, Jezewska MJ, Bujalowski W. Unzipping mechanism of the double-stranded DNA unwinding by a hexameric helicase. The effect of the 3′ arm and the stability of the dsDNA on the unwinding activity of the *Escherichia coli* DnaB helicase. J. Mol. Biol. 2004; 343:101–114. [PubMed: 15381423]
24. Jezewska MJ, Bujalowski W. A general method of analysis of ligand binding to competing macromolecules using the spectroscopic signal originating from a reference macromolecule. Application to *Escherichia coli* replicative helicase DnaB protein–nucleic acid interactions. Biochemistry. 1996; 35:2117–2128. [PubMed: 8652554]
25. Jezewska MJ, Rajendran S, Bujalowski W. Strand specificity in the interactions of *Escherichia coli* primary replicative helicase DnaB protein with replication fork. Biochemistry. 1997; 36:10320–10326. [PubMed: 9254631]
26. Jezewska MJ, Rajendran S, Bujalowski W. Functional and structural heterogeneity of the DNA binding of the *E. coli* primary replicative helicase DnaB protein. J. Biol. Chem. 1998; 3:9058–9069. [PubMed: 9535894]

27. Jezewska MJ, Rajendran S, Bujalowski W. Complex of *Escherichia coli* primary replicative helicase DnaB protein with a replication fork. Recognition and structure. Biochemistry. 1998; 37:3116–3136. [PubMed: 9485465]
28. Marcinowicz A, Jezewska MJ, Bujalowski PJ, Bujalowski W. The structure of the tertiary complex of the RepA hexameric helicase of plasmid RSF1010 with the ssDNA and nucleotide cofactors in solution. Biochemistry. 2007; 46:13279–13296. [PubMed: 17939681]
29. Bujalowski W, Jezewska MJ. Kinetic mechanism of the single-stranded DNA recognition by *Escherichia coli* replicative helicase DnaB protein. Application of the matrix projection operator technique to analyze stopped-flow kinetics. J. Mol. Biol. 2000; 295:831–852. [PubMed: 10656794]
30. Rajendran S, Jezewska MJ, Bujalowski W. Multiple-step kinetic mechanism of DNA-independent ATP binding and hydrolysis by *Escherichia coli* replicative helicase DnaB protein: quantitative analysis using the rapid quench-flow method. J. Mol. Biol. 2000; 303:773–795. [PubMed: 11061975]
31. Jezewska MJ, Rajendran S, Bujalowski W. *Escherichia coli* helicase PriA protein-single stranded DNA complex. J. Biol. Chem. 2000; 5:865–873.
32. Jezewska MJ, Rajendran S, Bujalowski W. Interactions of *Escherichia coli* replicative helicase PriA protein with single-stranded DNA. Biochemistry. 2000; 39:10454–10467. [PubMed: 10956036]
33. Galletto R, Jezewska MJ, Bujalowski W. Multi-step sequential mechanism of *E. coli* helicase PriA protein–ssDNA interactions. Kinetics and energetics of the active ssDNA-searching site of the enzyme. Biochemistry. 2004; 43:11002–11016. [PubMed: 15323559]
34. Ahnert P, Picha KM, Patel SS. A ring-opening mechanism for DNA binding in the central channel of the T7 helicase-primase protein. EMBO J. 2000; 19:3418–3434. [PubMed: 10880454]
35. Bujalowski W, Jezewska MJ, Galletto R. Dynamics of gapped DNA recognition by human polymerase β. J. Biol. Chem. 2002; 7:20316–20327. [PubMed: 11912205]
36. Bujalowski W, Jezewska MJ. Kinetic mechanism of nucleotide cofactor binding to *Escherichia coli* replicative helicase DnaB Protein. Stopped-flow kinetic studies using fluorescent, ribose-, and base-modified nucleotide analog. Biochemistry. 2000; 39:2106–2122. [PubMed: 10684661]
37. Galletto R, Bujalowski W. The *E. coli* replication factor DnaC protein exists in two conformations with different nucleotide binding capabilities. I. Determination of the binding mechanism using ATP and ADP fluorescent analogues. Biochemistry. 2002; 41:8907–8920. [PubMed: 12102633]
38. Galletto R, Bujalowski W. Kinetics of the *E. coli* replication factor DnaC protein-nucleotide interactions. II. Fluorescence anisotropy and transient, dynamic quenching stopped-flow studies of the reaction intermediates. Biochemistry. 2002; 41:8921–8934. [PubMed: 12102634]
39. Bujalowski W. Thermodynamic and kinetic methods of analyses of protein–nucleic acid interactions. From simpler to more complex systems. Chem. Rev. 2006; 106:556–606. [PubMed: 16464018]
40. Hammes, GG.; Schimmel, PR. The Enzymes. Kinetics and Mechanism. Vol. II. Academic Press; New York, NY: 1970. p. 67-114.
41. Hill, TL. Cooperativity Theory in Biochemistry. Steady State and Equilibrium Systems. Springer-Verlag; New York, NY: 1985. p. 167-234.
42. Epstein IR. Cooperative and non-cooperative binding of large ligands to a finite one-dimensional lattice. A model for ligand–oligonucleotide interactions. Biophys. Chem. 1978; 8:327–339. [PubMed: 728537]
43. McGhee JD, von Hippel PH. Theoretical aspects of DNA–protein interactions: cooperative and noncooperative binding of large ligands to a one-dimensional homogeneous lattice. J. Mol. Biol. 1974; 86:469–489. [PubMed: 4416620]
44. Bujalowski W, Lohman TM, Anderson CF. On the cooperative binding of large ligands to a one-dimensional homogeneous lattice: the generalized three-state lattice model. Biopolymers. 1989; 28:1637–1643. [PubMed: 2775853]
45. Fonseca MM, Scofano HM, Carvalho-Alves PC, Barrabin H, Mignaco JA. Conformational changes of the nucleotide site of the plasma membrane Ca^{2+}-ATPase probed by fluorescence quenching. Biochemistry. 2002; 41:7483–7489. [PubMed: 12044182]

46. Lakowicz, JR. Principles of Fluorescence Spectroscopy. 2nd edit.. Kluwer Academic; New York, NY: 1999. p. 185-233.
47. Connors, KA. Chemical Kinetics. The Study of Reaction Rates in Solution. VCH Publishers; New York, NY: 1990. p. 133-186.
48. Tanford, C. Physical Chemistry of Macromolecules. John Wiley & Sons, Inc.; New York, NY: 1961. p. 364-390.
49. Cantor, RC.; Schimmel, PR. Biophysical Chemistry. Vol. II. W. H. Freeman; New York, NY: 1980. p. 591-641.
50. Stafford W 3rd. Boundary analysis in sedimentation transport experiments: a procedure for obtaining sedimentation coefficient distributions using the time derivative of the concentration profile. Anal. Biochem. 1992; 203:295–301. [PubMed: 1416025]
51. Correia JJ, Chacko BM, Lam SS, Lin K. Sedimentation studies reveal a direct role of phosphorylation in Smad3:Smad4 homo- and hetero-dimerization. Biochemistry. 2001; 40:1473–1482. [PubMed: 11170475]
52. Galletto R, Jezewska MJ, Bujalowski W. Interactions of the *Escherichia coli* DnaB helicase hexamer with the replication factor the DnaC protein. Effect of nucleotide cofactors and the ssDNA on protein–protein interactions and the topology of the complex. J. Mol. Biol. 2003; 329:441–465. [PubMed: 12767828]
53. Galletto R, Maillard R, Jezewska MJ, Bujalowski W. Global conformation of the *Escherichia coli* replication factor DnaC protein in absence and presence of nucleotide cofactors. Biochemistry. 2004; 43:10988–11001. [PubMed: 15323558]
54. Lucius AL, Jezewska MJ, Bujalowski W. The *Escherichia coli* PriA helicase has two nucleotide-binding sites differing in their affinities for nucleotide cofactors. 1. Intrinsic affinities, cooperativities, and base specificity of nucleotide cofactor binding. Biochemistry. 2006; 45:7202–7216. [PubMed: 16752911]
55. Jezewska MJ, Rajendran S, Bujalowski W. Transition between different binding modes in rat DNA polymerase β–ssDNA complexes. J. Mol. Biol. 1998; 284:1113–1131. [PubMed: 9837730]
56. Otto R, Lillo MP, Beechem JM. Resolution of multi-phasic reactions by the combination of fluorescence total-intensity and anisotropy stopped-flow kinetic experiments. Biophys. J. 1994; 67:2511–2521. [PubMed: 7696490]
57. Jezewska MJ, Rajendran S, Bujalowska D, Bujalowski W. Does ssDNA pass through the inner channel of the protein hexamer in the complex with the *E. coli* DnaB helicase? Fluorescence energy transfer studies. J. Biol. Chem. 1998; 3:10515–10529. [PubMed: 9553111]
58. Galletto R, Jezewska MJ, Bujalowski W. Kinetics of allosteric conformational transition of a macromolecule prior to ligand binding. Analysis of stopped-flow kinetic experiments. Cell Biochem. Biophys. 2005; 42:121–144. [PubMed: 15858229]
59. Mulsch A, Colpan M, Wollny E, Gassen HG, Riesner D. Mechanism of the interactions between ribosomal protein S1 and oligonucleotides. Nucleic Acids Res. 1981; 9:2367–2385. [PubMed: 7019854]
60. Moore, JW.; Pearson, RG. Kinetics and Mechanism. J. Wiley & Sons; New York, NY: 1981. p. 192-234.
61. Edelhoch H. Spectroscopic determination of tryptophan and tyrosine in proteins. Biochemistry. 1967; 6:1948–1954. [PubMed: 6049437]
62. Gill SC, von Hippel PH. Calculation of protein extinction coefficients from amino acid sequence data. Anal. Biochem. 1989; 182:319–326. [PubMed: 2610349]
63. Pilar, FL. Elementary Quantum Chemistry. McGraw-Hill; New York, NY: 1968.
64. Fraser, RA.; Duncan, WJ.; Collar, AR. Elementary Matrices and Some Applications to Dynamics and Differential Equations. Cambridge University Press; New York, NY: 1965. p. 57-96.

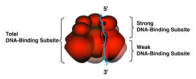

Fig. 1.

Schematic representation of the RepA hexamer, which shows orientation of the hexamer with respect to the polarity of the sugar-phosphate backbone of the nucleic acid in the complex with the ssDNA. The two front subunits are transparent to illustrate the cross channel of the hexameric structure and the locations of the strong and the weak DNA-binding subsites, within the total DNA-binding site of the enzyme on a single RepA subunit (see the text for details).[28]

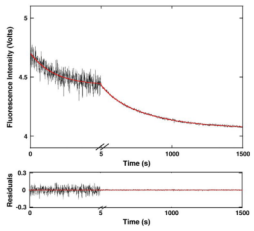

Fig. 2.

The fluorescence stopped-flow kinetic trace, recorded in two time bases, 5 and 1500 s, after mixing the ssDNA 21-mer, 5′-Fl-dT(pT)$_{19}$, with the RepA helicase in buffer T5 (pH 7.6, 10 °C), containing 0.5 mM AMP-PNP (λ_{ex} =475 nm, λ-$_{em}$ >500 nm). The final concentrations of the 21-mer and the helicase are 5×10^{-9} M (oligomer) and 5×10^{-7} M (hexamer), respectively. The continuous line is the three-exponential, nonlinear least-squares fit of the experimental curve using Eq. (10). The lower panel shows the deviations of the experimental curve from the fit.

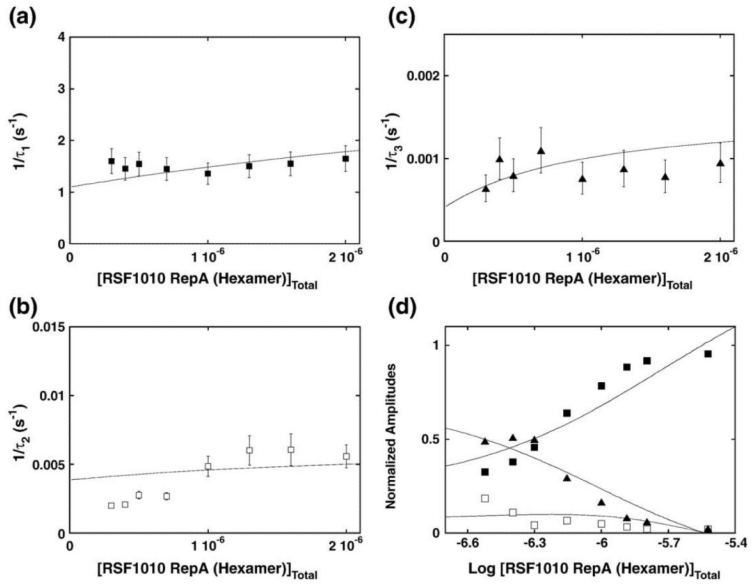

Fig. 3.

The dependence of the reciprocal of the relaxation times, $1/\tau_1$,$1/\tau_2$, and $1/\tau_3$, for the binding of the RepA hexamer to the ssDNA 21-mer, 5′-Fl-dT(pT)$_{19}$, in buffer T5 (pH 7.6, 10 °C), containing 0.5 mM AMP-PNP, upon the total concentration of enzyme. The continuous lines are nonlinear least-squares fits according to the four-step sequential mechanism, defined in Eq. (1), with the rate constants included in Table 1 (see the text for details); (a) $1/\tau_1$, (b) $1/\tau_2$, (c) $1/\tau_3$. The error bars are standard deviations obtained from three to four independent experiments. (d) The dependence of the normalized, individual relaxation amplitudes of the observed relaxation processes, A_1, A_2, and A_3, for binding of the RepA hexamer to the ssDNA 21-mer, 5′-Fl-dT(pT)$_{19}$, upon the logarithm of the total concentration of the RepA hexamer. The continuous lines are nonlinear least-squares fits according to the four-step sequential mechanism, defined in Eq. (1), with the relative fluorescence intensities included in Table 1. The rate constants are the same as those obtained from the relaxation time analysis (Table 1); A_1, ■; A_2, □; A_3, ▲.

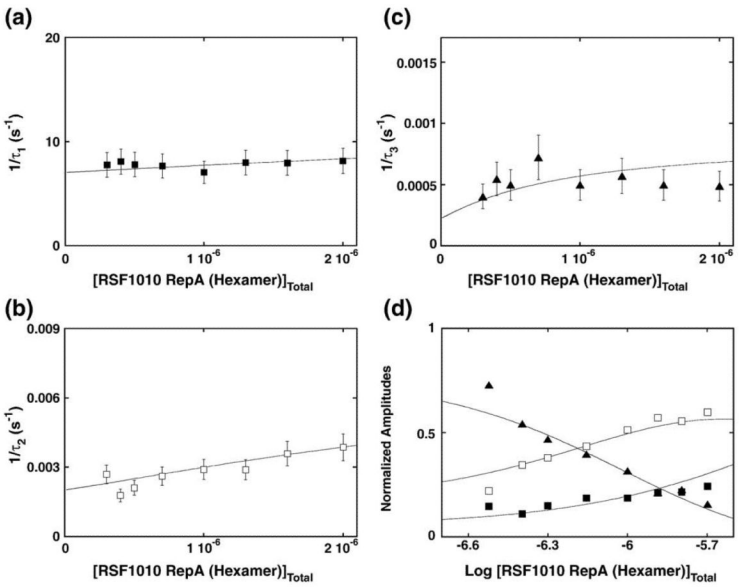

Fig. 4.

The dependence of the reciprocal of the relaxation times, $1/\tau_1$, $1/\tau_2$, and $1/\tau_3$, for the binding of the RepA hexamer to the ssDNA 10-mer, 5′-Fl-dT(pT)$_8$, in buffer T5 (pH 7.6, 10 °C), containing 0.5 mM AMP-PNP, upon the total concentration of enzyme. The continuous lines are nonlinear least-squares fits according to the four-step sequential mechanism, defined in Eq. (1), with the rate constants included in Table 2 (see the text for details); (a) $1/\tau_1$, (b) $1/\tau_2$, (c) $1/\tau_3$. The error bars are standard deviations obtained from three to four independent experiments. (d) The dependence of the normalized, individual relaxation amplitudes of the corresponding relaxation processes, A_1, A_2, and A_3, for binding of the RepA hexamer to the ssDNA 10-mer, 5′-Fl-dT(pT)$_8$, upon the logarithm of the total concentration of the RepA hexamer. The continuous lines are nonlinear least-squares fits according to the four-step sequential mechanism, defined in Eq. (1), with the relative fluorescence intensities included in Table 2. The rate constants are the same as those obtained from the relaxation time analysis (Table 2); A_1, ■; A_2, □; A_3, ▲.

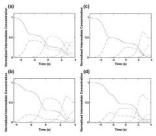

Fig. 5.

Computer simulation of the time course of the fractional concentration distribution of different ssDNA species, in the binding to the RepA hexamer helicase to the ssDNA 21-mer, 5′-Fl-dT(pT)$_{19}$, using the determined rate constants included in Table 1, in buffer T5 (pH 7.6, 10 °C), containing 0.5 mM AMP-PNP, at two different temperatures: (a) 10 °C and (b) 20 °C; the analogous plots of the fractional concentration distributions of different ssDNA species, in the binding to the RepA hexamer helicase to the ssDNA 11-mer, 5′-Fl-dT(pT)$_9$, using the determined rate constants included in Table 2, at two different temperatures: (c) 10 °C and (d) 20 °C. The total ssDNA oligomer concentrations are 5×10^{-9} M (oligomer). The selected RepA helicase concentration is 5×10^{-6} M (hexamer). Free ssDNA oligomer, —; (H-ssDNA)$_1$, — — —; (H-ssDNA)$_2$, — - —; (H-ssDNA)$_3$, — - - - —; (H-ssDNA)$_4$, – – –.

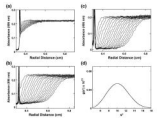

Fig. 6.

(a) Absorption profiles, recorded at 495 nm, of analytical sedimentation velocity runs of the ssDNA 11-mer, 5′-Fl-dT(pT)$_9$, alone in buffer T5 (pH 7.6, 10 °C) and in the presence of 0.5 mM AMP-PNP. The total nucleic acid concentration is 5×10^{-6} M. (b) Absorption profiles, recorded at 495 nm, of analytical sedimentation velocity runs of the ssDNA 11-mer, 5′-Fl-dT(pT)$_9$, in the presence of the RepA Helicase, in buffer T5 (pH 7.6, 10 °C), containing 0.5 mM AMP-PNP. The total nucleic acid and protein concentrations are 5×10^{-6} M and 8×10^{-6} M (hexamer), respectively. (c) Absorption profiles, recorded at 495 nm, of analytical sedimentation velocity runs of the ssDNA 21-mer, 5′-Fl-dT(pT)$_{19}$, in the presence of the RepA Helicase, in buffer T5 (pH 7.6, 10 °C) and in the presence of 0.5 mM AMP-PNP. The total nucleic acid and protein concentrations are 5×10^{-6} M and 8×10^{-6} M (hexamer), respectively. All scans were collected at 35,000 rpm. (d) The continuous line is the apparent average sedimentation coefficient distribution, $g(s^*)$, as a function of the radial sedimentation coefficient coordinate, s^*, obtained from time derivatives of the RepA hexamer-5′-Fl-dT(pT)$_{19}$ complex sedimentation profiles recorded at 495 nm, in buffer T5 (pH 7.6, 10 °C) containing 0.5 mM AMP-PNP; 35,000 rpm. The broken line is the nonlinear least-squares fit of the experimental distribution using the time-derivative method. Both plots are corrected for the solution conditions (for details, see the text).

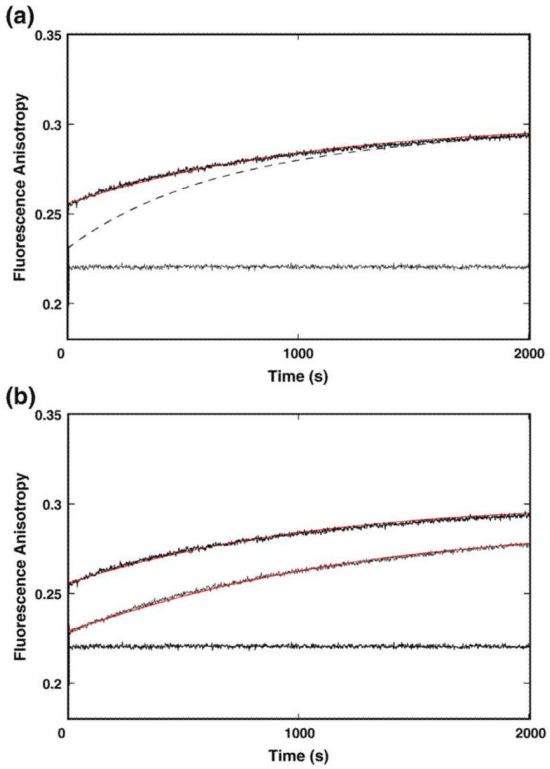

Fig. 7.

(a) The fluorescence anisotropy stopped-flow kinetic trace, recorded at a single time base, after mixing the ssDNA 21-mer, 5′-Fl-dT(pT)$_{19}$, with the RepA helicase in buffer T5 (pH 7.6, 20 °C), containing 0.5 mM AMP-PNP (λ_{ex} = 475 nm, λ_{em} > 500 nm). The final concentrations of the 21-mer and the helicase are 5 × 10 $^{-9}$ M (oligomer) and 1 × 10^{-6} M (hexamer), respectively. The continuous red line is the nonlinear least-squares fit of the experimental curve using the four-step kinetic mechanism, defined in Eq. (8), with the rate constants and fluorescence intensities of the intermediates taken from Table 1 and the steady-state anisotropies of the intermediates: r_{D0} = 0.225, r_{D1} = 0.400, r_{D2} = 0.290, r_{D3} = 0.290, and r_{D4} = 0.340 (see the text for details). The time course of the steady-state anisotropy of the nucleic acid alone is included in the panel. The broken line is the best fit of the observed fluorescence anisotropy kinetic curve using the three-step, sequential kinetic mechanism, with the rate constants k_1 = 2.0 × 10^5 M^{-1} s^{-1} k_{-2} = 1.9 s^{-1}, k_2 = 0.015 s^{-1}, k_{-2} = 0.0005 s^{-1}, k_3 = 0.0002 s^{-1}, and k_{-3} = 0.004 s^{-1} and relative fluorescence intensities F_0 = 1, F_1 = 0.1, F_2 = 0.9, and F_3 = 0.86 and r_{D0} = 0.230, r_{D1} = 0.300, r_{D2} = 0.300, and r_{D3} = 0.380 (see the text for details). (b) The fluorescence anisotropy stopped-flow kinetic traces, recorded at a single time base, after mixing the ssDNA 21-mer, 5′-Fl-dT(pT)$_{19}$, with the RepA helicase at two different concentrations of the enzyme (hexamer): 7 × 10^{-7} M and 1 × 10^{-6} M, respectively. The continuous red lines are the nonlinear least-squares fit of the experimental curve using the four-step kinetic mechanism, defined in Eq. (8), with the rate constants and fluorescence intensities of the intermediates taken from Table 1, with the steady-state anisotropies of the intermediates for the protein concentration 1 × 10^{-6} M (r_{D0} = 0.225, r_{D1} = 0.400, r_{D2} = 0.290, r_{D3} = 0.290, and r_{D4} = 0.340) and for the protein concentration 7 × 10^{-7} M (r_{D0} = 0.203, r_{D1} = 0.405, r_{D2} = 0.0, r_{D3} = 0.3, and r_{D4} = 0.365) (see the text for details).

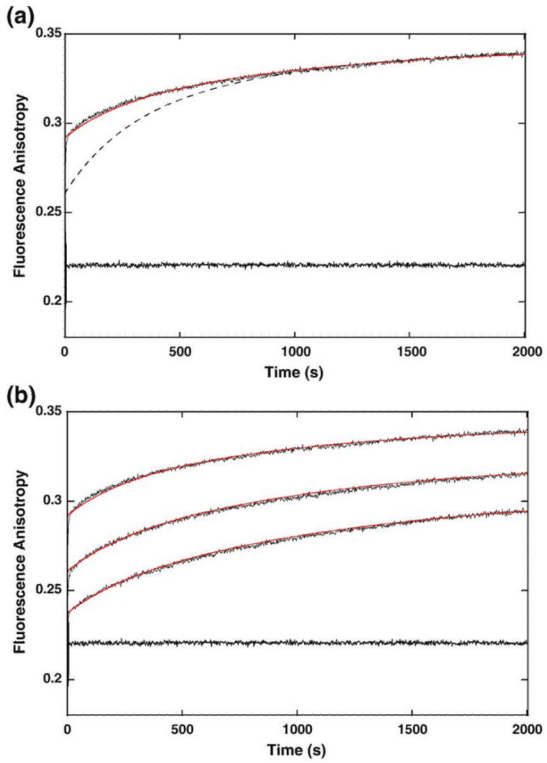

Fig. 8.

(a) The fluorescence anisotropy stopped-flow kinetic trace, recorded at a single time base, after mixing the ssDNA 21-mer, $dT(pT)_{19}$-Fl-3′, with the RepA helicase in buffer T5 (pH 7.6, 10 °C), containing 0.5 mM AMP-PNP (λ_{ex} = 475 nm, λ_{em}>500 nm). The final concentrations of the 21-mer and the helicase are 5×10^{-9} M (oligomer) and 1×10^{-6} M (hexamer), respectively. The continuous red line is the nonlinear least-squares fit of the experimental curve using the four-step kinetic mechanism defined in Eq. (8), with the rate constants and fluorescence intensities of the intermediates taken from Table 1 and the steady-state anisotropies of the intermediates: r_{D0} = 0.241, r_{D1} = 0.420, r_{D2} = 0.370, r_{D3} = 0.370, and r_{D4} = 0.365 (see the text for details). The time course of the steady-state anisotropy of the nucleic acid alone is included in the panel. The broken line is the best fit of the observed fluorescence anisotropy kinetic curve using the three-step, sequential kinetic mechanism, with the rate constants $k_1 = 2.0 \times 10^5$ M^{-1} s^{-1}, k_{-1} = 1.3 s^{-1}, k_2 = 0.02 s^{-1}, k_{-2} = 0.001 s^{-1}, k_3 = 0.0005 s^{-1}, and k_{-3} = 0.0007 s^{-1} and relative fluorescene intensities F_0 = F_1 = F_2 = F_3 = 1 and r_{D0} = 0.240, r_{D1} = 0.400, r_{D2} = 0.337, and r_{D3} = 0.400 (see the text for details). (b) The fluorescence anisotropy stopped-flow kinetic traces, recorded at a single time base, after mixing the ssDNA 21-mer, Fl-$dT(pT)_{19}$-Fl-3′, with the RepA helicase at three different concentrations of the enzyme (hexamer): 5×10^{-7}, 7×10^{-7}, and 1×10^{-6} M, respectively. The continuous red lines are the nonlinear least-squares fit of the experimental curve using the four-step kinetic mechanism, defined in Eq. (8), with the rate constants and fluorescence intensities of the intermediates taken from Table 1 and steady-state anisotropies of the intermediates for the protein concentration 1×10^{-6} M (r_{D0} = 0.241, r_{D1} = 0.420, r_{D2} = 0.370, r_{D3} = 0.370, and r_{D4} = 0.365), 7×10^{-7} M (r_{D0} = 0.217, r_{D1} = 0.410, r_{D2} = 0.360, r_{D3} = 0.360, and r_{D4} = 0.370), and 5×10^{-7} M (r_{D0} = 0.205, r_{D1} = 0.380, r_{D2} = 0.343, r_{D3} = 0.360, and r_{D4} = 0.371) (see the text for details).

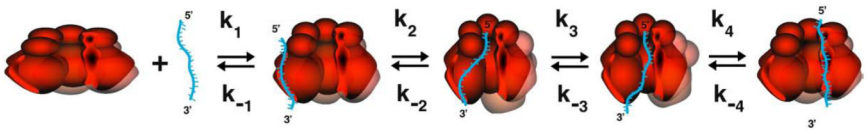

Fig. 9.

Schematic model for the binding of the ssDNA to the total DNA-binding site, the RepA hexamer. The DNA binds initially to the outer DNA-binding site of the helicase on one of the subunits, forming the initial complex, $(H\text{-}ssDNA)_1$.In the intermediate $(H\text{-}ssDNA)_1$, local conformational transition of the complex strongly immobilizes the entire nucleic acid. The hexameric structure of the enzyme remains closed. In the next intermediate, $(H\text{-}ssDNA)_2$, the hexamer partially and locally opens and the part of the bound nucleic acid, from its 5′ end, enters the cross channel, although the DNA cannot yet engage the total DNA-binding site inside the cross channel. The DNA fragment in the vicinity of the 3′ end stays bound to the outer DNA-binding site. In the following intermediate, $(H\text{-}ssDNA)_3$, the opening of the hexameric structure widens without significantly affecting the state of the bound DNA, allowing the entire DNA to enter the cross channel. In the final intermediate, $(H\text{-}ssDNA)_4$, the nucleic acid is completely in the cross channel and forms all contacts with the total DNA-binding site located inside the cross channel. The hexameric structure closes over the bound DNA, although, possibly, only partially (see the text for details).

Table 1

Thermodynamic, kinetic, and spectroscopic parameters of the binding of the RepA hexameric helicase of plasmid RSF1010 to different ssDNA oligomers that occlude the total DNA-binding site, in buffer T5 (pH 7.6), containing 0.5 mM AMP-PNP, at different temperatures (see the text for details)

ssDNA oligomer	K_1 (M^{-1})	K_2	K_3	K_4	k_2 (s^{-1})	k_{-2} (s^{-1})	k_3 (s^{-1})	k_{-3} (s^{-1})	k_4 (s^{-1})	k_{-4} (s^{-1})	F_1	F_2	F_3	F_4	F_{max}[a]
10 °C 5′Flu-dT(pT)$_{19}$	(1.5 ± 0.7) × 10^5	2.7 ± 1.0	2.5 ± 2.3	1.9 ± 1.0	3.0 ± 0.5	1.1 ± 0.2	(5.0 ± 1.0) × $^{-3}$	(2.0 ± 0.2) × 10^{-3}	(1.5 ± 0.3) × 10^{-3}	(8.0 ± 1.5) × 10^{-4}	1.05 ± 0.03	0.65 ± 0.03	0.84 ± 0.03	0.84 ± 0.03	0.79 ± 0.03
20 °C 5′Flu-dT(pT)$_{19}$	(5 ± 1.6) × 10^4	8.0 ± 2.6	6.3 ± 2.3	0.8 ± 0.3	12 ± 2.4	1.5 ± 0.3	(5.0 ± 1.0) × 10^{-3}	(8.0 ± 1.6) × 10^{-4}	(3.0 ± 0.5) × 10^{-4}	(4.0 ± 0.9) × 10^{-4}	1.00 ± 0.03	0.60 ± 0.03	0.86 ± 0.03	0.82 ± 0.03	0.82 ± 0.03
10 °C 5′Flu-dT(pT)$_{24}$	(1.0 ± 0.3) × 10^5	2.3 ± 0.8	3.8 ± 1.3	3.8 ± 1.3	3.0 ± 0.5	1.3 ± 0.2	(3.0 ± 0.5) × 10^{-2}	(8.0 ± 1.5) × 10^{-3}	(1.5 ± 0.3) × 10^{-3}	(4.0 ± 0.7) × 10^{-4}	1.00 ± 0.03	0.20 ± 0.03	0.76 ± 0.03	0.62 ± 0.03	0.63 ± 0.03
10 °C 5′Flu-dT(pT)$_{29}$	(1.0 ± 0.3) × 10^5	2.5 ± 0.8	3.8 ± 1.3	4.0 ± 1.3	3.0 ± 0.5	1.2 ± 0.2	(3.0 ± 0.6) × 10^{-2}	(8.0 ± 1.5) × 10^{-3}	(1.2 ± 0.2) × 10^{-3}	(3.0 ± 0.6) × 10^{-4}	1.00 ± 0.03	0.18 ± 0.03	0.70 ± 0.03	0.68 ± 0.03	0.66 ± 0.03
20 °C 5′Flu-dT(pT)$_{29}$	(5.0 ± 1.6) × 10^4	5.6 ± 1.8	5 ± 1.6	2 ± 0.6	9.5 ± 1.9	1.7 ± 0.3	(1.5 ± 0.3) × 10^{-2}	(3.0 ± 0.6) × 10^{-3}	(8.0 ± 1.5) × 10^{-4}	(4.0 ± 0.8) × 10^{-4}	1.00 ± 0.03	0.24 ± 0.03	0.78 ± 0.03	0.67 ± 0.03	0.68 ± 0.03

Errors are standard deviations determined using three to four independent experiments.

[a] Determined in equilibrium fluorescence titrations.

Table 2

Thermodynamic, kinetic, and spectroscopic parameters of the binding of the RepA hexameric helicase of plasmid RSF1010 to ssDNA oligomers that occlude only the strong DNA-binding subsite in buffer T5 (pH 7.6), containing 0.5 mM AMP-PNP, at different temperatures (see the text for details)

Oligomer	K_1 (M^{-1})	K_2	K_3	K_4	k_2 (s^{-1})	k_{-2} (s^{-1})	k_3 (s^{-1})	k_{-3} (s^{-1})	k_4 (s^{-1})	k_{-4} (s^{-1})	F_1	F_2	F_3	F_4	F_{max}[a]
10 °C 5′Flu-dT(pT)$_7$	$(5.0 \pm 1.6) \times 10^4$	1.4 ± 0.4	15.4 ± 5.1	0.8 ± 0.2	20 ± 4	14.5 ± 2.9	$(4.0 \pm 0.8) \times 10^{-2}$	$(2.6 \pm 0.5) \times 10^{-3}$	$(6.0 \pm 1.2) \times 10^{-4}$	$(8.0 \pm 1.6) \times 10^{-4}$	1.0 ± 0.03	0.70 ± 0.03	0.77 ± 0.03	0.81 ± 0.03	0.78 ± 0.03
10 °C 5′Flu-dT(pT)$_s$	$(7.5 \pm 2.8) \times 10^4$	1.4 ± 0.4	11.5 ± 3.7	1.7 ± 0.5	15.0 ± 3	7.1 ± 1.4	$(1.7 \pm 0.3) \times 10^{-2}$	$(1.2 \pm 0.1) \times 10^{-3}$	$(5.0 \pm 1) \times 10^{-4}$	$(3.0 \pm 0.6) \times 10^{-4}$	1.0 ± 0.03	0.30 ± 0.03	0.54 ± 0.03	0.62 ± 0.03	0.60 ± 0.03
0 °C 5′Flu-dT(pT)$_s$	$(4.0 \pm 1.3) \times 10^4$	3.3 ± 1.1	7.3 ± 2.4	1.0 ± 0.3	200 ± 50	60 ± 12	$(3.3 \pm 0.6) \times 10^{-2}$	$(4.5 \pm 0.9) \times 10^{-3}$	$(1.5 \pm 0.3) \times 10^{-3}$	$(1.5 \pm 0.3) \times 10^{-4}$	1.0 ± 0.03	0.55 ± 0.03	0.70 ± 0.03	0.53 ± 0.03	0.62 ± 0.03
10 °C 5′Flu-dT(pT)$_9$	$(2.0 \pm 0.6) \times 10^5$	0.71 ± 0.26	16 ± 5	0.83 ± 0.07	2.7 ± 0.5	3.8 ± 0.7	$(1.6 \pm 0.5) \times 10^{-2}$	$(1.0 \pm 1.5) \times 10^{-3}$	$(5.0 \pm 0.4) \times 10^{-4}$	$(6.0 \pm 1.5) \times 10^{-4}$	1.0 ± 0.03	0.73 ± 0.03	0.71 ± 0.03	0.45 ± 0.03	0.61 ± 0.03
0 °C 5′Flu-dT(pT)$_9$	$(7.0 \pm 2.3) \times 10^4$	2.2 ± 0.7	10.5 ± 3.5	0.44 ± 0.11	48 ± 9	22 ± 4	$(2.1 \pm 0.4) \times 10^{-2}$	$(2.0 \pm 0.4) \times 10^{-3}$	$(4.0 \pm 0.8) \times 10^{-4}$	$(9.0 \pm 1.8) \times 10^{-4}$	1.0 ± 0.03	0.84 ± 0.03	0.84 ± 0.03	0.45 ± 0.03	0.73 ± 0.03

Errors are standard deviations determined using three to four independent experiments.

[a] Determined in equilibrium fluorescence titrations.

Table 3

van't Hoff's enthalpies and entropies characterizing the formation of intermediates in the binding of the RepA hexameric helicase of plasmid RSF1010 to different ssDNA oligomers that occlude the strong DNA-binding subsite or the total DNA-binding site of the enzyme, in buffer T5 (pH 7.6), containing 0.5 mM AMP-PNP (see the text for details)

ssDNA oligomer	ΔH_1 (kcal/mol)	ΔS_1[a] (cal/mol deg)	ΔH_2 (kcal/mol)	ΔS_2[a] (cal/mol deg)	ΔH_3 (kcal/mol)	ΔS_3[a] (cal/mol deg)	ΔH_4 (kcal/mol)	ΔS_4[a] (cal/mol deg)
5′Flu-dT(pT)$_8$	−10 ± 5	−14 ± 7	14 ± 7	51 ± 27	−7 ± 3	−22 ± 12	−9 ± 5	−30 ± 15
5′Flu-dT(pT)$_9$	−17 ± 8	−37 ± 18	19 ± 9	65 ± 35	−7 ± 3	−19 ± 9	−11 ± 6	−37 ± 19
5′Flu-dT(pT)$_{19}$	−18 ± 9	−40 ± 21	18 ± 9	65 ± 35	15 ± 8	55 ± 33	−15 ± 7	−52 ± 31
5′Flu-dT(pT)$_{29}$	−11 ± 6	−18 ± 8	13 ± 7	49 ± 26	5 ± 2	19 ± 10	−11 ± 6	−38 ± 19

Errors are standard deviations determined using three to four independent experiments.

[a] Calculated using the binding constant determined at 10 °C.